INVESTIGATION OF SOLIDIFICATION OF HIGH-STRENGTH STEEL CASTINGS

AMMRC CR 63-04/F

FINAL REPORT

for

October 1, 1966 - December 31, 1967

by

T. Z. Kattamis and M. C. Flemings

July 15, 1968

Department of Metallurgy and Materials Science
Massachusetts Institute of Technology
Cambridge, Massachusetts 02139

Contract No. DA-19-020-AMC-5443(X)
D/A Project No. 1C024401A328
AMCMS CODE 5025.11.294

Metals Research for Army Materiel

Army Materials and Mechanics Research Center
Watertown, Massachusetts 02172

ABSTRACT

The morphology, size and distribution of sulfide inclusions are studied in vacuum melted and solidified AISI 4330 low alloy steel deoxidized with various elements such as Al, Si, Mn, either individually or in various combinations, and B, Zr and Ce. Types I, II and III inclusions are investigated in detail. Type I inclusions are isolated, roughly spherical sulfides, Type II inclusions have an interconnected rod-like morphology, and Type III inclusions are angular and unconnected (except they are often connected to Type II inclusions).

Effects of chemistry (Al, Si, Mn) on inclusion Type is quantitatively determined. The effect of cooling rate on inclusion type and size is examined for a few cases. With decreasing cooling rate, the average size of Type I inclusions and the average spacing of the eutectic Type II inclusions increase.

The origin of the various types of inclusions observed is interpreted with the aid of the Fe-MnS pseudo-binary phase diagram and the Fe-Mn-S ternary phase diagram. Modifications of these diagrams from addition of the various deoxidizers are qualitatively predicted and taken into account. It is concluded that Type I inclusions form by exsolution of liquid sulfide pools from the melt, Type III inclusions form by solidification of sulfide crystals out of the melt and Type II inclusions form by eutectic solidification of the sulfur-rich final liquid. Interpretation of structures observed suggests that Type I and possibly Type III inclusions are "pushed" ahead of growing dendrites. Morphology of inclusions is adequately predicted on the basis of only temperature and mode of solidification; such factors as surface energy differences between different inclusion types need not be postulated to explain their different morphologies.

TABLE OF CONTENTS

LIST OF FIGURES

CHAPTER I - INTRODUCTION

Research has been conducted on solidification of steel castings at Massachusetts Institute of Technology since late 1958. Research in the years 1958-1963 was on foundry techniques for improving the mechanical properties of steel castings. Techniques were developed, including "unidirectional solidification", for achieving major improvements in properties. Several of the more general papers describing this work are referenced[1-6].

Work in the period 1963-1967 concentrated on study of structural variables known to influence properties of steel castings. Detailed fundamental studies were conducted on formation of microsegregation in steel castings. Extensive comparison of theory with experiment was made. Homogenization kinetics were studied, and compared with theory; these studies led to the important works of Quigley and Ahearn[7] and others showing the major improvements in properties in low alloy steel obtainable from high temperature homogenization treatments. Microporosity was studied and techniques developed for its evaluation that have become useful industry tools. This work has been summarized in four reports and seven technical papers[8-18].

Research on this program since late 1967 has been primarily on another structural variable known to be strongly influential on properties of steel castings; inclusions. Work has been on inclusion formation and growth, and on influences of inclusion morphology and chemistry on mechanical properties; this is the first report dealing with that work. Work currently in progress on effects of inclusions on mechanical properties will be summarized in a later report. Initial work, and that reported herein, has been primarily on developing a

fundamental understanding of influence of solidification variables on morphology of sulfide inclusions. Work has been both experimental and theoretical - theoretical work being primarily on detailed description of segregation and solidification in multicomponent ferrous alloys (e.g., Fe-Mn-S).

CHAPTER II - LITERATURE SURVEY

A significant amount of work has been published on the morphology and effect on mechanical properties of sulfide inclusions in iron, low and medium carbon steel and low alloy steel[19-47]. Wentrup[19] studied the formation of inclusions in the iron-sulfur (Fe-FeS), iron-sulfur-oxygen (Fe-FeO-FeS), iron-manganese-sulfur (Fe-FeS-MnS-Mn) and iron-manganese-oxygen-sulfur (FeO-MnO-FeS-MnS) systems. Vogel et al[20] studied the iron-manganese-sulfur system in more detail, published several sections of this ternary diagram, and proposed the pseudobinary iron-manganese sulfide diagram. Both Wentrup[19] and Vogel et al[20] found various sulfide morphologies analogous to the sulfide types later defined by Sims[22] and Sims and Briggs[23]. These authors examined the effects of various deoxidizers on the morphology of sulfide inclusions in low and medium carbon steels in the as-cast condition. Deoxidizers studied were: manganese, aluminum, titanium, zirconium, and misch metal. They found that, in normal steels containing more than 0.5 percent manganese, sulfides are essentially MnS and can be classified briefly as Types I, II, and III.

Type I inclusions are randomly dispersed spheres having a wide range of sizes; Type II inclusions appear as chains or stringers along grain boundaries and Type III inclusions appear as randomly scattered, faceted crystals. Type II inclusions are highly undesirable leading to a material of poor ductility, Type I inclusions lead to a substantially more ductile material and Type III inclusions are not as desirable as Type I but are certainly preferable to Type II, for a given sulfur level[23]. Manganese, though a weak deoxidizer, was found to improve the action of stronger deoxidizers like aluminum and silicon when present[22].

Aluminum is a powerful deoxidizer but not as powerful as zirconium. Small additions of aluminum may be sufficient for deoxidation but lead to Type II inclusions. Larger additions of aluminum are necessary to obtain Type III inclusions. Titanium above 0.015 percent leads to Type II inclusions, Type III inclusions are not obtained no matter how much titanium is added. Zirconium, on the other hand, leads to Types II or III according to the amount added to the melt. Misch metal converts Types II and III sulfides (formed by additions of aluminum and zirconium) back to Type I. However, it has no effect on Type II inclusions obtained by deoxidizing the melt with titanium[23].

Sims has attempted to explain the formation of Type III sulfide inclusions by surface tension considerations[22]. He assumed an excess of aluminum or zirconium increased the sulfide-matrix interfacial energy, resulting in shrinkage and formation of liquid pools at regions where more than two grain boundaries meet. Schürmann studied in great detail the Fe-FeS-MnS-Mn phase diagram and its modification when carbon is added to the system[21]. Van Vlack et al[24] examined the dependence of the microstructure of sulfide inclusions upon steel composition and analyzed the behavior of sulfides at steel rolling temperatures. The effects of morphology and composition of sulfide inclusions on hot-shortness of steel and on improvement of machinability were also studied, and the effect of the sulfur level on the surface quality of hot-rolled steel stressed[24].

The nature, composition and physical properties (mainly microhardness) of sulfide inclusions, both real and synthetic, of the (Mn, Me)S type (where Me is a transition metal of the first long period like chromium, titanium, vanadium or iron) were extensively studied by Kiessling et al [25-28] and were correlated with the composition of the base-metal. The importance of the hardness and

plasticity of inclusions and of the depletion of the matrix around them with respect to deformability and machinability of the matrix was stressed[25]. Some types of duplex sulfide-oxide or sulfide-silicate inclusions were examined[26]. Composition studies of (Mn, Fe)S inclusions were also reported by Matsubara[29]. Boulger[30] examined the effect of sulfur and selenium on the machinability and tensile properties of a 5 percent chromium steel. Gaydos[31] investigated the effects of sulfide and siliceous inclusions in free-machining steels. He examined the nature of duplex inclusions as a function of their position in the ingot and correlated it to the oxygen level in the steel at that particular position. Detrez[32,33] redefined the three types of sulfide inclusions in steels and found that the critical aluminum levels for the transition between Types I and II, and II and III to occur depend on the sulfur, oxygen, and therefore carbon levels. With a high sulfur level (above 0.1 percent) and a very low carbon level (below 0.05 percent) it was found almost impossible to obtain Type III sulfide inclusions. Detrez[32,33] studied also the Charpy impact strength of steel as a function of the existing type of sulfide inclusions.

Araki et al[34] studied the nature and plastic behavior of sulfide inclusions during forging of a resulfurized low carbon steel containing chromium and molybdenum. Melford[35] applied x-ray scanning microanalysis to study the composition of duplex sulfide inclusions in high chromium steel. Lichy et al[36] studied the control of sulfide shape after rolling in low carbon aluminum-killed steel. They found that the heavy stringer sulfides occurring in non-zirconium bearing steel after rolling were changed into an interesting oval type when zirconium 0.10-0.18 percent was present. Bäcker et al[37] examined the nature and composition of sulfide inclusions in resulfurized cast steel having an

improved machinability. They also investigated the distribution of elements like manganese throughout the specimen, namely inside the matrix, the carbide inclusions, the sulfide inclusions and the oxides. Kondo et al[38] studied briefly the composition of inclusions in resulfurized high-speed steel and Araki et al[39] conducted similar studies on the effect of molybdenum, carbon and other elements on sulfide inclusions in low carbon steel. Salmon Cox et al[40] examined the nature, type and distribution of sulfides and duplex sulfide-silicate inclusions across an ingot of 0.2 percent carbon steel. They found that Type I randomly dispersed sulfide inclusions containing also a silicate phase are more frequent in the columnar and branched regions of the ingot, whereas Type II eutectic inclusions were more frequent in the equiaxed region of the ingot. They concluded that the silicate phase has been rejected from limited solid solution with the sulfide as opposed to Karmazin[41] who postulated that the silicate phase is in fact a particle acting as nucleating agent of the sulfide.

The interrelationship between FeS and MnS inclusions was examined by Whiteley[42]. Nicodemi[43] examined the morphology and the effect of cooling rate on non-metallic inclusions in stainless steel castings. He observed that the size of sulfides or duplex oxide-sulfide inclusions decreases with increasing cooling rate. Analogous observations were made by other investigators[34,44] who noticed the coarsening of sulfide particles with distance from the ingot edge. Yeo[45] studied the effect of oxygen content and deoxidation by silicon, boron, aluminum and carbon in resulfurized steels on sulfide morphology and machinability. He found that sulfide inclusions are hardened by oxygen during rolling, so that they remain more globular. Dahl et al[46] investigated in detail the conditions of occurrence of the various types of sulfide inclusions in low carbon steel and the effect of various deoxidizers and attempted an

explanation of the various morphological observations on the inclusions based on the phase diagram of the system.

The effect on inclusions of the variation in initial oxygen content has been recognized and studied by Crafts and Hilty[47]. These authors examined in detail the structure of inclusions in the iron-oxygen-sulfur system as well as in the system modified by additions of manganese, aluminum, and silicon.

CHAPTER III - EXPERIMENTAL PROCEDURE

Several series of cylindrical ingots (1.1" dia. x 1.1" high) were prepared of AISI 4330 low alloy steel whose nominal composition is given in Table I. In these ingots the sulfur level was generally brought up to 0.1 percent. Deoxidation was conducted using various deoxidizers as indicated in Table II. Melting and solidification were conducted in a Balzer USG 10 vacuum induction unit with a 30 KW, 10 KC power source. Samples were heated indirectly using a graphite susceptor. Specimens of AISI 4330 steel weighing approximately 100 gms. were loaded in fused silica crucibles together with the corresponding amount of sulfur added as pure FeS, and in some cases with the adequate amount of deoxidizer. The system was melted under 1/2 atmosphere of argon superheated to approximately 1585°C (corresponding to about 100°C superheat), held isothermally for 10 minutes in order to homogenize the melt and subsequently cooled down first at an average rate of 15°C/min. by decreasing the power, and later on, at the onset of nucleation of the matrix, at a rate of about 70°C/min. by shutting off the power. Undercooling before nucleation of the steel was intentionally prevented by nucleating the melt with an iron wire.

Deoxidizers, such as Mn, and Si, do not react appreciably with the silica crucible. They were added to the system during the melt-down period. Deoxidizers like Al, Zr, B which react with the silica crucible were added at the end of the isothermal holding period and were allowed to dissolve and react during the slow cooling period prior to nucleation of the melt. One or two weighed pieces of the deoxidizer were fastened on a pure iron rod by means of pure iron wire. The rod was lowered into the melt at the appropriate moment. Because the time available for reaction is short, no appreciable reaction is believed to occur

between silica crucible and deoxidizer. Temperature was measured and recorded using a Pt/Pt-10 percent Rh thermocouple and a Moseley Autograf strip chart recorder.

Specimens thus prepared were polished and examined metallographically, generally unetched but in some cases etched with Rosenhain's reagent. This etchant, used for observing the dendritic structure, consists of an aqueous solution of copper, iron and stannous chlorides. Some specimens were studied using electron microanalysis. Inclusions were also examined by x-ray scanning analysis.

Measurement of volume percent of inclusions was done by quantitative metallography. A two-dimensional systematic point count was used following procedure of Cahn and Hilliard[48]. A systematic array of points was used, provided by corners of a two-dimensional 10 x 10 grid having 100 points. The grid was traced on the metallograph on which the photomicrograph is projected.

A coarse-mesh lattice criterium is the following:

$$p_o + p_1 = 1$$

$$p_n = 0 \text{ for } n \geq 2$$

where p_n is the probability that a feature will occupy n lattice points.

Inclusion diameter measurements were carried out by making a number of random traverses across photomicrographs of the sample, counting the number of inclusions, N_L, crossed by the line and measuring the total length of line L intercepted by the inclusions. The mean lineal intercept, $\overline{L}$, was obtained from $\overline{L} = (L/N_L)$.

The average spacing, $\bar{L}$, of Type II inclusions was measured by drawing a line through the center of the inclusions and measuring the number of inclusions, N_L, intercepted per unit length of line. The average spacing, $\bar{L}$, is then given by $\bar{L} = (1/N_L)$.

CHAPTER IV - RESULTS

The metallographic observations made on various etched and unetched specimens may be summarized as follows:

Series I. AISI 4330 Specimens Containing Various Amounts of Sulfur

Specimens of AISI 4330 low alloy steel were prepared containing 0.01, 0.02, 0.05, 0.1, 0.2, 0.5 and 1.0 percent. As expected, it was observed that the volume fraction of sulfides increases with increasing amount of sulfur. The type of inclusions is mixed; there is a coexistence of Type I and II inclusions. Inclusions of Type I are individual spheres or spheroids of a wide size distribution scattered in the interdendritic spaces, Figure 1a, Type II inclusions appear as rosaries of beads or chains, or stringers, along grain boundaries. It is sometimes difficult to distinguish between Type I and Type II inclusions by examining a single polished surface. Ambiguity is eliminated by successively polishing down the specimen and examining the new surfaces. Figure 1b is a typical photomicrograph of a specimen containing 0.1 percent S, showing the coexistence of the two types of inclusions.

With increasing amount of sulfur, there is an obvious shifting of inclusion type from I to II, Figure 2. Inclusion type is close to I in the specimen containing 0.01 percent S and close to II in that containing 1.0 percent S. Because of the coexistence of inclusions of Types I and II the structure may be characterized by a number such as the "relative volume fraction of Type II and Type I inclusions." Thus, when the relative volume fraction of Type II inclusions is higher than 90 percent, the specimen is said herein to present Type II sulfides. If the relative volume fraction of Type II inclusions is lower than 10 percent, the specimen is said to present Type I sulfides.

With increasing sulfur level, the size of inclusions increases. At high magnification, they appear to consist of two phases identified as (Mn,Fe)S and FeS*. Inclusions in specimens containing more than 0.05 percent S appear to have silicate or oxide cores which increase in size with sulfur level and inclusion size.

Because the sulfur level has such a significant effect on the type of inclusions, specimens in which the effect of various deoxidizers was studied were made with a constant sulfur content, namely 0.1 percent. The advantage of this value is that for this sulfur level the sulfide morphology is quite analogous to that expected in non-resulfurized AISI 4330 steel specimens. Conclusions based on morphological observations made on specimens containing 0.1 percent S may, therefore, be extrapolated to non-resulfurized specimens.

The bulk of the work reported in subsequent sections (on effect of various deoxidizers on inclusion morphology) was conducted on 0.1 percent S melt. Detailed examination of the morphology of Type II inclusions in specimens containing 0.1 percent S shows, first, an alignment of beads and stringers, Figure 3. Polishing down and examining the successive surfaces reveals that in fact the beads and stringers are interconnected at some level; Figure 3 shows several of a large number of such sections studied. The morphology of the sulfides as a group is that of a degenerate eutectic[49], very similar to that of a "chinese scriptum" consisting of irregularly cylindrical rods. Thus, for this particular case, the classical "beads" are in reality intersections of "stringers" by the polishing plane. Figure 4 shows the same area of this specimen etched and unetched. It appears clearly that eutectic inclusions are spread along dendrite

* In reflected natural light (Mn,Fe)S has a dove gray color, whereas FeS has a very light gray color.

arm boundaries and not along grain boundaries as generally supposed. Figure 5 represents schematically the morphology of the eutectic Type II inclusions around a dendrite arm.

The examination of the samples containing various amounts of sulfur showed that with increasing distance from the ingot edge or from a cooling surface the size of inclusions increases and that there is a progressive shifting of inclusion morphology towards Type I. In order to study more schematically these observations, a series of four ingots of AISI 4330 steel containing 0.1 percent were solidified at four different cooling rates, 70, 40, 20, and 10°C/min by adequately adjusting the power during the cooling period. Figure 6 shows the decrease in average diameter of Type I inclusions (measured by lineal analysis) versus increasing cooling rate. Figure 7 shows the decrease in eutectic rod diameter and in average eutectic spacing with increasing cooling rate. The variation of spacing is plotted in Figure 8.

Series II. AISI 4330 Specimens Containing 0.1 Percent Sulfur and Various Amounts of Oxygen

Two ingots were solidified containing more oxygen than would correspond to equilibrium with the silica crucible at the isothermal holding temperature. The oxygen was added to the melt as Fe_2O_3 of known analysis. In one ingot, 0.04 percent oxygen was added; the inclusion resulting type was mixed I-II. At the center of the ingot the inclusions were over 90 percent Type I and at the edge they were over 90 percent Type II. In the other ingot, 0.08 percent oxygen was added; inclusions were Type I. Sulfides contain dark oxide cores, Figure 9.

Series III. AISI 4330 Specimens Containing 0.1 Percent Sulfur and Deoxidized with Various Amounts of Aluminum

Five AISI 4330 ingots were made containing 0.05, 0.3, 0.4, 0.5, and 0.8 percent Al respectively. Aluminum was added to the melt at the end of the isothermal holding period. At up to 0.3 percent Al additions, the type of inclusions was mixed I-II. Beyond this level, inclusions were essentially of Type II. No traces of Type III inclusions were observed with Al additions as high as 0.8 percent as would be expected from work by Sims[23] and Sims and Briggs[24] on low and medium carbon steel.

Series IV. AISI 4330 Specimens Containing 0.1 Percent Sulfur and Various Amounts of Aluminum and Silicon

A series of 16 ingots of AISI 4330 were made, containing 0.1 percent S and various amounts of Al and Si, Table II. A metallographic examination of the Type of inclusions led to the compilation of points in Figure 10. Three curves are shown, dividing the space of the quadrant into four regions. In the first region, corresponding to very low Si and Al contents, inclusions are of mixed Type I-II. In the second region, corresponding to low Al and Si content, inclusions are of Type II. In the third region, corresponding to higher Al and Si contents, inclusions are mixed Type II-III, Figure 11. In the fourth region corresponding to still higher Al and Si contents, the relative volume fraction of Type III inclusions exceeds 90 percent and the type of sulfides is then defined as III. Type III inclusions appear as intersections of idiomorphic cubic crystals with the plane of polishing. They seem scattered throughout the dendritic structure but are mainly concentrated in the interdendritic spaces. A close study of these inclusions shows that: (1) their cubic patterns are often disturbed by "dendritic" projections, and (2) they often surround regions of Type II inclusions and project

arms which join these interdendritic eutectic networks. (3) They often appear cracked, Figure 12.

Series V. AISI 4330 Specimens Containing 0.1 Percent Sulfur and Various Amounts of Aluminum and Manganese

A series of seventeen ingots of AISI 4330 specimens were made containing 0.1 percent S and various amounts of Al and Mn, Table II. Figure 13 summarizes metallographic observations relating to the resulting inclusion type. For very low Mn and Al additions, inclusions are of the mixed Type I-II. For low Mn and Al additions, they are of Type II, for higher Mn and Al additions, they are of mixed Type II-III and for still higher additions they are of Type III.

Series VI. AISI 4330 Specimens Containing 0.1 Percent Sulfur and Various Amounts of Silicon and Manganese

Six AISI 4330 ingots were prepared containing 0.1 percent S and deoxidized with various amounts of Si and Mn. Figure 14 shows that for very low Mn and Si contents, inclusions are of mixed Type I-II, whereas for higher contents they are of Type II. For high Mn and Si contents, a mixed Type II-III is obtained. For compositions as high as 1 percent Mn and 1 percent Si, inclusions are still of the mixed Type II-III.

Photomicrographs of a polished specimen of this series, containing 0.1 percent S-0.3 percent Si are given in Figure 15. An apparently new type of inclusions can be seen. They are globular, ring-like with a matrix core, similar to Type I inclusions. Type II and Type III inclusions lie next to them. Type II inclusions of this specimen, observed at high magnification, exhibit an internal eutectic structure, Figure 16.

Series VII. AISI 4330 Specimens Containing 0.1 Percent Sulfur and Various Amounts of Silicon, Manganese, and Aluminum

The information included in Figures 10, 13, and 14 was compiled in a three-dimensional geometric representation of the compositional regions in which mixed Type I-II, Type II, mixed Type II-III and Type III of inclusion may be expected, Figure 17.

The curves shown are approximate since experimental points have been obtained to date only along the three orthogonally oriented planes. Additional work is currently in progress on alloy compositions within the space enclosed by the three axes. To date, three ingots have been made with all three elements (Si, Mn, Al) present, Table II.

Series VIII. AISI 4330 Specimens Containing 0.1 Percent Sulfur, a High Oxygen Concentration and Various Amounts of Silicon, Aluminum, and Manganese

Three ingots of AISI 4330 containing 0.1 percent S were made. The oxygen level was increased by addition of 0.02 percent Oxygen as Fe_2O_3. The amounts of Al, Si, and Mn added were the same as those added in the three ingots of the previous series VII. Thus, the compositions of the two series of ingots differed only by their respective oxygen levels. Series VII contained approximately 0.008 percent oxygen and Series VIII approximately 0.02 percent Oxygen. The effect on inclusion morphology of this oxygen content increase is that the type of inclusions in the high oxygen ingots is mixed II-III instead of III. This shows clearly that an increase of oxygen content moves the surfaces between regions II and II-III on one hand, and between regions II-III and III on the other, towards higher values of Al, Si, and Mn. A similar effect can logically be expected by decreasing the carbon level of this steel.

Series IX. AISI 4330 Specimens Containing 0.1 Percent Sulfur and Deoxidized with Either Zirconium, Boron, Cerium

Additions of 0.4 percent Zr to an AISI 4330 steel ingot containing 0.1 percent S leads to Type III sulfide inclusions. Low additions of 0.05 percent Zr do not seem to affect the inclusion Type and morphology. Additions of 0.1 percent Ce or misch metal to the same allow convert Type II inclusions into Type I. Additions of only 0.05 percent B do not affect the Type of inclusions. These morphological changes will be described in more detail below:

Specimen Containing 0.4 Percent Zirconium

Photomicrographs of the polished and unetched specimen are given in Figure 18. Type III sulfides appear as idiomorphic hexagonal crystals, Figures 18a and b, scattered mainly between dendrite arms and occasionally within the dendrites themselves. Type II sulfides appear as elongated stringers along interdendritic spaces. By successively polishing down and examining a large number of sections it has been found that in reality these stringers are narrow lamellae, often attached to Type II inclusions. In addition, the similarity of optical properties (such as color in natural and polarized light and index of refraction) of crystals and lamellae indicate that presumably these two Types of sulfides have very nearly the same composition. Preliminary electron microprobe examination has shown that these inclusions contain about 20 percent Zr besides Mn and S. Some Type III inclusions present a dark core, Figure 18b, which is quite probably a zirconium silicate. Idiomorphic zirconium silicate crystals appear scattered in certain regions of the specimen, Figure 18d.

Specimen Containing 0.3 Percent Boron

Photomicrographs of this specimen are given in Figure 19. The dendritic structure appears readily without etching,Figure 19(a), because of significant

eutectic formation in the interdendritic spaces. This eutectic involves an (Fe, Mn, Cr, Ni, Mo) phase and an (Fe, Mn, Cr, Ni, Mo) boride phase. Coring inside the dendrite arms appears by etching lightly the specimen with Marble's reagent, Figure 19b. Type III inclusions consisting of idiomorphic crystals are scattered in the interdendritic spaces, mainly along dendrite arm boundaries. The relative position of these sulfides with respect to the eutectic appears clearly in Figures 19c and d.

Specimen Containing 0.1 Percent Cerium

Photomicrographs of this specimen are given in Figure 20. Sulfide inclusions belong to Type I. They are globular and are scattered between dendrite arms. More than one phase appears inside the inclusions. The very dark phase is presumably an oxide or a silicate containing Ce, the dark-gray phase is a cerium-rich sulfide (CeS) and the light dove gray phase is the usual Mn-rich sulfide. In addition, as in Figure 20 d, some of the iron-rich matrix material occasionally appears within the inclusion.

Series X. AISI 4330 Specimens Containing 0.5 Percent Sulfur and Various Amounts of Manganese and Silicon

Photomicrographs of the specimen containing 2 percent Mn are given in Figure 21. Some regions of the specimen exhibit the structure analogous to that of Figure 21a. The inclusion Type is mixed II-III. Type II inclusions are scattered at sites where two or three boundaries meet. Other regions of the specimen exhibit the structure of Figure 21b. Here, there is a continuous and wide network of eutectic sulfide inclusions along the dendrite arm boundaries.

Figure 22 shows photomicrographs of the specimen containing 2 percent Mn-0.3 percent Si. Type II inclusions form wide eutectic networks between

dendrite arm boundaries. These networks are surrounded by Type III inclusions appearing as idiomorphic crystals often with arms projecting inside the eutectic regions.

CHAPTER V - DISCUSSION

The origin and solidification behavior of the various types of sulfide inclusions in the AISI 4330 low alloy steel will be discussed in the present Chapter. Low alloy steel being a rather complex chemical system, simplifications will be made in order that available phase diagrams be used for understanding the solidification process.

The various types of sulfide inclusions encountered in the present study are basically (Mn, Fe)S solid solutions; the average oxygen concentration of the melts, approximately 0.003 percent (30 ppm), was low enough that oxygen is reasonably neglected in discussing this multicomponent system. It is, therefore, logical that the analytical examination of the Fe-Mn-S system be the backbone of the discussion to follow.

Figure 23 shows schematically the Fe-Mn-MnS-FeS part of the Fe-Mn-S phase diagram. The four sides of the diagram are the binaries: Fe-FeS, Fe-Mn, Mn-MnS, and MnS-FeS[20,28,50]. The Fe-FeS phase diagram is a simple eutectic diagram with practically no iron solid solubility in iron sulfide. The solid solubility of sulfur in iron is as low as 0.2 percent[51] at room temperature. The Mn-MnS phase diagram presents a eutectic, G, near the manganese side, a liquid miscibility gap, DK'E, and a monotectic, E, near the MnS side. The FeS-MnS phase diagram is a eutectic type with no solid solubility of manganese in iron sulfide and a significant solid solubility of iron in manganese sulfide. The Fe-Mn binary is one of nearly complete solid solubility with narrow liquid-solid region. The liquidus and solidus are simplified to a single line in Figure 24 for clarity.

The liquid miscibility gap KMNCDK'EOK has the shape of an oblong dome of crest-line $\overline{KK'}$ limited by the contour EOKMNCD. The projection of this contour

on the basal plane of the diagram illustrates the slopes of its various segments. Thus, K is a minimum point whereas C and P, intersections of the contour with the vertical plane whose trace on the basal plane is the diagonal Fe-MnS, are maximum points. The segment $\overline{EO}$ is a monotectic valley whereas $\overline{OH}$, $\overline{LH}$, and $\overline{QH}$ are eutectic valleys converging towards H, the ternary eutectic. $\overline{QG}$ is also a eutectic valley descending from Q, a maximum point situated in the same vertical plane as P and C, to G, the binary eutectic.

The basal plane projection of the monotectic and eutectic valleys and of the limiting contour of the liquid miscibility gap are also shown schematically in Figure 24. Figure 25a shows some tie lines across the miscibility gap, leaning against the contour of the gap[21]. Figure 25b shows the shift of the miscibility gap, of the tie lines across the gap and of the eutectic valleys when carbon is added to the Fe-Mn-S system[21]. The configuration of the two basal projections of the systems Fe-Mn-S and Fe(C)-Mn-S being similar, conclusions formulated by studying the solidification behavior of the first system should be qualitatively applicable to the second.

Figure 26 represents schematically the pseudobinary phase diagram Fe-MnS obtained by sectioning the ternary Fe-Mn-S phase diagram by the vertical plane whose trace on the basal plane is the diagonal Fe-MnS. This pseudobinary is used below for a simplified interpretation of the origin and solidification behavior of the various types of sulfide inclusions. A second and more rigorous way of conducting this investigation is by using the basal projections of Figures 25a, 27, and 28.

Experimental observations made in this study, and which may be understood at least qualitatively by the discussion to follow using the phase diagrams of Figures 23-26, include the following:

(1) Type I inclusions appear as spheres of wide size distribution, scattered randomly in interdendritic spaces (not throughout the whole matrix as widely believed). It is possible, though rare, to see a few such inclusions within the dendrites.

(2) Type II inclusions appear as a eutectic-like network of irregular cylindrical rods spread along interdendritic spaces (not just along grain boundaries as widely believed). The classical "beads" and "stringers" are random intersections of the eutectic network by the polishing plane.

(3) Type III inclusions appear as idiomorphic crystals scattered throughout the whole dendritic structure, but frequently situated in interdendritic spaces. They often project arms which join Type II inclusions.

(4) More than one type inclusion is generally observed in a given sample, but some Type II is found in all specimens.

(5) Increasing sulfur content favors formation of Type II inclusions.

(6) For an alloy containing 0.1 percent S certain chemical variables favor the following transitions:

(a) Increasing amounts of Al favor Type I → Type II

(b) Increasing amounts of Al and Mn and/or Si favor Type II→ Type III

(c) Decrease in O level favors Type I→Type II

(d) Decrease in O level and increase in Al, Mn and/or Si levels favor Type II→Type III

(e) Addition of Zr or B favors Type II→Type III

(f) Ce additions favor Type II→Type I

For qualitative interpretation of the foregoing, consider first several alloys within the pseudobinary Fe-MnS system. Since, as noted in Figure 25 and elsewhere[21], tie lines during solidification lie approximately within this pseudobinary, we need only consider the binary when examining solidification of alloys whose composition initially lies along the line joining Fe and MnS; this pseudobinary is sketched in Figure 26.

The binary of Figure 26 will be used to discuss solidification of three different alloys (Alloys 1, 2, and 3 of Figure 26), making the essential pre-suppositions that (1) MnS-rich liquid (L_2) comprises Type I inclusions, (2) the eutectic Type II inclusions form at the eutectic Q as $L_1 \rightarrow$ Fe + MnS(solid) and (3) Type III inclusions form from the melt L_1 as $L_1 \rightarrow$ MnS(solid); the equilibrium temperature range for this reaction lies above the eutectic Q and below the eutectic P. The second pre-supposition has been made earlier by Sims[22]. Recently, Dahl et al[46] made all three pre-suppositions.

Consider, first, solidification of alloy 1, Figure 26, whose liquidus is L_1. Assuming negligible undercooling before nucleation, iron-rich dendrites will nucleate at T_{L_1} and grow while the liquid composition moves from L_1 to the

eutectic composition Q. At T_Q, the eutectic Fe-MnS forms (eutectic Type II inclusions). This alloy, solidified in this manner, will consist of only Type II inclusions in an iron matrix.

Next, consider alloy 2, also solidifying with negligible undercooling of all phases before nucleation. Here, solid Type III inclusions nucleate at L_1' and grow while the liquid moves to the eutectic Q. Final structure consists of Type III and Type II inclusions, with the proportion of Type II inclusions decreasing as initial liquid composition moves from Q towards C.

Next, consider Alloy 3, also solidifying with negligible undercooling of all phases before nucleation. Liquid Type I sulfides grow above the eutectic temperature of liquid L_2; solid Type III sulfides grow at lower temperatures but above the eutectic of L_1, and eutectic Type II sulfides grow at the eutectic of liquid L_1 (at Q). Hence, this alloy, as solidified, contains Types I, II, and III sulfides.

Finally, if nucleation of solid MnS is supposed to be hindered in any one of the three alloys discussed above, a different combination of inclusion types will result. As example, consider Alloy 1. Suppose nucleation of solid MnS cannot occur at Q, but liquid L_2 forms at T_Q'. Thus, Type I inclusions form and provided solid MnS later nucleates, Type II sulfides may also form after recalescence at or near T_Q. Similarly Alloy 2 will comprise Type I, II and III or Types I and II according to the maximum recalescence temperature reached [52].

The foregoing simple discussion explains qualitatively the bulk of the observations made in this work, including the general morphological features

of different types of inclusions. One exception is the fact that (assuming no undercooling before nucleation) inclusions of Types I and III form before the solid iron dendrites, and would therefore be expected to be distributed more or less at random, not concentrated preferentially at dendrite arm boundaries. The observed concentration at dendrite boundaries is presumably due to one or both of the following factors:

(1) After inclusion formation, and during growth and coarsening of dendrites, inclusions are pushed ahead of the liquid-solid interface into interdendritic spaces. This "pushing" has been demonstrated for SiO_2 inclusions in an iron alloy[53].

(2) The Type I inclusions form, not according to the equilibrium diagram, but after formation of some primary iron phase as discussed above. Perhaps "hollow" inclusions as shown in Figure 15 are found in this way.

The pseudobinary phase diagram may also be used to qualitatively explain the modification of inclusion type for a given steel melt, by addition of a deoxidizer, and its amount used. Assume , as example, that deoxidation with silicon lowers the equilibrium liquidus lines as indicated schematically in Figure 25b; the melt of composition 1 which in absence of silicon gave Type II inclusions will now lead to a mixed Type II-III inclusions. There is sufficient evidence that such a shifting of the equilibrium liquidus might take place[54]. More systematic research is necessary for quantitative information about this shifting.

For alloys whose initial composition is not exactly in the binary Fe-MnS, the multicomponent diagram of Figures 23-25 must be used to study solidification

(or, for convenience, the schematic basal projections of Figures 27 and 28).

Consider first the melt $\mathcal{L}$ of hypoeutectic composition, Figure 27. Now assuming no undercooling before nucleation, the liquid composition follows the heavy path shown in Figure 27 during solidification. Solid iron dendrites nucleate at the equilibrium liquidus, and the liquid moves along the straight line $\overline{A\mathcal{L}B}$ (since solid solubility of sulfur is negligible). At B, eutectic Type II inclusions nucleate and grow as liquid composition moves toward the ternary eutectic point H. Final structure comprises only Type II inclusions in the iron matrix.

The solidification behavior of melt $\mathcal{L}$ of slightly hypereutectic composition lying in the field of primary sulfide crystallization, Figure 28a may be summarized as follows (negligible undercooling): When the temperature of the melt reaches the equilibrium liquidus, solid manganese sulfide crystals nucleate. With decreasing temperature the liquid as well as the solidifying sulfide become richer in iron. When the liquid composition reaches B on the eutectic valley, iron nucleates and the eutectic Type II sulfides grow, either by new nucleation, or by extension of the already existing primary sulfides. The solidification is again completed when the ternary eutectic H is reached. The resulting inclusion type is mixed II-III (e.g., Figures 11, 18, and 22).

When the composition of the melt $\mathcal{L}$ falls inside the liquid miscibility gap, Figure 19b, the solidification process is quite different. As soon as the dome is reached, pools of a sulfide rich liquid L_2 separate out of the melt of composition L_1. With decreasing temperature L_1 and L_2 move

in opposite directions and L_1 reaches point a_1 when L_2 reaches point a_2, $\overline{a_2a_1}$ forming a tie line. While the temperature decreases further, the liquid L_{a_2} moves along the monotectic line $\overline{PO}$ whereas the melt L_{a_1} moves along the line $\overline{CN}$. L_{a_2} comprises the sulfide-rich Type I inclusions forming as a liquid from the melt. Now, according to simple equilibrium solidification considerations L_{a_2} gives monotectically liquid L_{a_1} + solid (Mn,Fe)S and the liquid is entirely consumed by the monotectic reaction. However, it should be recognized that as with the case of the discussion on the simple binary, the Type I sulfides comprise a very small volume fraction of the total melt, and after the iron dendrites begin to grow, these sulfides must be very quickly surrounded and trapped. Hence, any changes that occur to liquid L_2 during cooling from $a_2 \rightarrow b_2$ will be localized within these isolated pools, will not change the shape of the sulfides (Type I) significantly, and will result in no overall change in inclusion chemistry.

The other liquid, L_1, comprises a significantly larger volume fraction than does L_2. As this liquid cools along $\overline{b_1B}$, Type III sulfides grow, and as it proceeds along BH, Type II sulfides grow. At the completion of solidification at H, the resulting inclusion type is mixed I-II-III, Figure 15, Type I being the inclusions which separated as liquid pools and solidified between a_2 and b_2, III being the inclusions which solidified out of the melt as sulfide crystals between b_1 and B, and II being the eutectic inclusions which solidified along the eutectic valley $\overline{BH}$.

Figure 28c deals with another case of a melt $\mathcal{L}$ whose composition falls inside the miscibility gap. The solidification process is quite similar to that

examined in the previous case, except that $\overline{b_1 B}$ is zero in the present case. Thus, when the liquid L_2 is completely consumed at b_2 by the monotectic reaction, any subsequent decrease in temperature causes nucleation of the eutectic out of the melt L_{b_1} which then is at point B. There are no primary sulfide crystals in this case. The final inclusion type is mixed I-II, Figure 1b.

In the case of the ternary system, as in the pseudobinary system discussed earlier, the range of possible structures is increased if the possibility of hindered nucleation of Type II sulfides is considered. However, in all cases, it is predicted that Type II eutectic inclusions should be present to at least some small extent in all specimens of the analyses considered. It could be repeated that for a given steel melt, the type of inclusions to be expected depends on the position of the various curves in the basal projection. These curves shift according to the nature and the amount of deoxidizer used as illustrated in Figure 26b for the case of carbon.

Solidification considerations based on the basal projection method provide a possible explanation to various observations relating to the effect of cooling rate on the type and size of inclusions. It was observed that a slower solidification decreased the relative volume fraction of Type II inclusions in specimens presenting a mixed Type I-II.

In all the systems discussed herein, oxygen, as an element, was not taken into account. The analysis of cases in which oxide or silicate cores appear in sulfide inclusions should, however, consider oxygen as well. These cases are illustrated by Figures 9 and 2. The presence of oxide or silicate core in Type I inclusions, Figure 9, is to be expected because, in this specimen, the

oxygen level was intentionally raised by addition of Fe_2O_3. The presence of oxide in the high sulfur specimens, Figure 2, could also be expected because it is well known[55] that with increasing sulfur levels the equilibrium solubility of oxygen in molten steel increases.

CHAPTER VI - CONCLUSIONS

1. Sulfide inclusions in AISI 4330 vacuum melted and solidified low alloy steel may be classified into three types, I, II, and III. Type I inclusions appear as individual spheroids of a wide size distribution scattered randomly in the interdendritic spaces (not through the whole matrix as widely believed). Type II inclusions appear as a degenerate eutectic network made of irregular cylindrical rods, spread out in the interdendritic spaces, delineating the dendrite arm boundaries (not just at grain boundaries as widely believed). The classical "beads" and "stringers" observed are in reality intersections of a eutectic network by the polishing plane. Type III inclusions appear as idiomorphic crystals scattered through the whole dendritic structure, but with a higher frequency in the interdendritic spaces. More than one type of inclusion usually coexist in a given sample. The usual occurrences are: Type II, mixed Type I-II, mixed Type II-III, and mixed Type I-II-III.

2. The sulfide inclusions in the AISI 4330 specimens (with no other addition) are of a mixed Type I-II and consist of a (Mn, Fe, Cr)S solid solution. With increasing S content the volume fraction of sulfide inclusions increases and there is a morphological shifting towards Type II. With increasing amount of O, there is a reverse shifting towards Type I inclusions.

3. In ingots deoxidized with Al, there is a shifting towards inclusion Type II with increasing amount of Al. No Type III inclusions are observed by addition of Al alone.

4. A simultaneous deoxidation of the melt with Al and Si, or Al and Mn, or Al, Si and Mn may lead to formation of Type III inclusions. A three-dimensional

compositional diagram has been plotted, allowing the determination of those combinations of Al, Si and Mn contents which lead to a particular type of inclusions. An increase in the O level displaces the various limiting surfaces of the diagram in such a way that higher amounts of Al, Si and Mn are required for obtaining Type III inclusions. The opposite conclusion is expected to be valid with an increasing C level.

5. Cerium used as a deoxidizer causes a shifting of the inclusion Type towards I. Zirconium additions lead to a mixed Type II-III sulfide inclusion containing approximately 20 percent Zr. The Type III inclusions appear as idiomorphic crystals scattered in the dendritic structure, but mainly concentrated in the interdendritic spaces projecting arms which join the Type II inclusions. Boron additions lead to a mixed Type of inclusions which is nonetheless very close to Type III. Idiomorphic crystals appear scattered almost exclusively in the interdendritic spaces occupied by a matrix-boride eutectic.

6. With increasing amounts of S and Mn, the Type II eutectic network becomes wider. It is surrounded by Type III inclusions often showing dendritic tendencies with projections joining the eutectic network.

7. With decreasing cooling rate, the relative volume fraction of Type I inclusions and their average size increases. The average spacing of the eutectic Type II inclusions also increases. For very low solidification rates, the Type II eutectic network degenerates into isolated rods or spheroids.

8. In a specimen cast with mixed Type I-II-III inclusions, Type I inclusions appear to be ring-like. This particular morphology is attributed to undercooling.

9. The origin of the various Types of inclusions has been explained by following the solidification process of the deoxidized alloy on the Fe-Mn-S ternary phase diagram, or, for greater convenience, on the pseudo-binary Fe-MnS phase diagram. The modification of these diagrams by addition of the various deoxidizers is expected to be responsible for the morphological variation of the inclusions observed. It is concluded that Type I inclusions form by exsolution of sulfide pools out of the steel melt, Type III inclusions form by solidification of sulfide crystals out of the melt, and Type II inclusions form by solidification of the sulfur-rich liquid along a eutectic valley. Morphologies of the different types of inclusions are explained on the basis of phase diagram considerations alone, without need of postulating, for example, differences in surface energy behavior of the different inclusion types. However, to rationalize the final distribution of inclusions observed, it is suggested that Type I, and to a lesser extent, Type III inclusions are "pushed" by growing dendrites.

TABLE I

Nominal Composition of AISI 4330
Low Alloy Steel

C	0.31
Ni	1.83
Cr	0.95
Mn	0.86
Mo	0.44
Si	0.27
Va	0.08
Fe	Balance

TABLE II

Specimens Prepared and Type of Inclusions Observed

	Composition	Cooling Rate °C/min	Type of Inclusions
Series I	AISI 4330+0.01S	40	I-II towards I
	0.02S	40	I-II towards I
	0.05	40	I-II towards I
	0.1S	70	I-II intermediate
	0.1S	40	I-II intermediate
	0.1S	20	I-II towards I
	0.1S	10	I-II almost I, coarser
	0.2S	40	I-II intermediate
	0.5S	40	I-II intermediate
	1.0S	40	Almost II
Series II	AISI 4330+0.1S+0.04 0	40	I-II. At center of ingot, Type I, at the edge, Type II, smaller size
	0.08 0	40	I. Dark oxide cores
Series III	AISI 4330+0.1S+0.05Al	40	I-II
	0.3Al	40	I-II
	0.4Al	40	Almost II
	0.5Al	40	II
	0.8Al	40	II. No traces of III
Series IV	AISI 4330+0.1S+0.05Si+0.1Al	40	I-II
	0.1Si+0.1Al	40	II
	0.1Si+0.2Al	40	II
	0.05Si+0.3Al	40	II
	0.5Si,0.1Si	40	II, I-II
	0.2Si+0.1Al	40	II-III
	0.2Si+0.3Al	40	II-III
	0.1Si+0.35Al	40	II-III
	0.5Si+0.1Al	40	II-III
	0.9Si	40	II-III
	0.2Si+0.4Al	40	III
	0.3Si+0.3Al	40	III
	0.4Si+0.2Al	40	III
	0.5Si+0.3Al	40	III
	0.7Si+0.1Al	40	III

TABLE II (continued)

Series V	AISI 4330+0.1S+0.05Mn+0.1Al	40	I-II
	0.1Mn+0.1Al	40	II
	0.1Mn+0.2Al	40	II
	0.1Mn+0.3Al	40	II
	0.2Mn+0.1Al	40	II
	0.1Mn+0.5Al	40	II-III
	0.2Mn+0.2Al	40	II-III
	0.2Mn+0.4Al	40	II-III
	0.3Mn+0.3Al	40	II-III
	0.05Mn	40	I-II
	0.4Mn+0.1Al	40	II-III
	1.4Mn	40	II-III
	0.3Mn+0.5Al	40	III
	0.4Mn+0.3Al	40	III
	0.5Mn+0.2Al	40	III
	0.7Mn+0.4Al	40	III
	0.85Mn+0.1Al	40	III
Series VI	AISI 4330+0.1S+0.3Si+0.3Mn	40	II
	0.3Si+0.7Mn	40	II
	0.45Si+0.5Mn	40	II
	0.40Si+0.7Mn	40	II-III
	0.5Si+0.5Mn	40	II-III
	1.0Si+1.0Mn	40	II-III
Series VII	AISI 4330+0.1S+0.1Si+0.5Mn+0.4Al	40	III
	0.2Si+0.3Mn+0.3Al	40	III
	0.5Si+0.4Mn+0.1Al	40	III
Series VIII	AISI 4330+0.1S+0.02 0+0.1Si+0.5Mn+0.4Al	40	II-III
	0.2Si+0.3Mn+0.3Al	40	II-III
	0.5Si+0.4Mn+0.1Sl	40	II-III
Series IX	AISI 4330+0.1S+0.4Zr	40	III
	0.3B	40	III
	0.1Ce	40	I
Series X	AISI 4330+0.5S+2Mn	40	II-III
	0.5S+2Mn+0.3Si	40	II-III

CHAPTER VI - REFERENCES

1. M. C. Flemings, D. Peckner, "Premium Quality Castings", Materials in Design Engineering, August, 1963, pp. 99-106.

2. M. C. Flemings, R. V. Barone, S. Z. Uram, H. F. Taylor, "Solidification of Steel Castings and Ingots", Transactions AFS, v. 69, 1961, pp. 422-435.

3. M. C. Flemings, "Stronger, Tougher Steel Castings", Materials in Design Engineering, September, 1962, pp. 93-96.

4. G. E. Nereo, R. F. Polich, M. C. Flemings, "Unidirectional Solidification of Steel Castings", Transactions AFS, v. 73, 1965, pp. 1-13.

5. R. F. Polich, M. C. Flemings, "Mechanical Properties of Unidirectional Steel Castings", Transactions AFS, v. 73, 1965, pp. 28-33.

6. M. C. Flemings, "Directional Solidification", Proceedings Fourteenth Sagamore Army Materials Conference, Syracuse University Press (to be published).

7. F. C. Quigley, P. J. Ahearn, "Homogenization of Steel Castings at 2500°F.", Transactions AFS, v. 72, 1964, pp. 813-817.

8. R. Barone, H. D. Brody, M. C. Flemings, "Investigation of Solidification of High Strength Steel Castings", Army Materials Research Agency, Contract No. DA-19-020-ORD-5443(X), October, 1964.

9. D. Poirier, M. C. Flemings, "Investigation of Solidification of High Strength Steel Castings", Army Materials Research Agency, Contract No. DA-19-020-ORD-5443(X), October, 1965.

10. R. Barone, H. D. Brody, M. C. Flemings, "Investigation of Solidification of High Strength Steel Castings", Army Materials Research Agency, Contract No. DA-19-020-ORD-5443(X), October, 1966.

11. T. Z. Kattamis, M. C. Flemings, "Solidification of Iron Base Alloys", Army Materials and Mechanics Research Center, Contract No. DA-19-020-ORD-5443(X), Final Report, September, 1966-January, 1968.

12. A. Tzavaras, M. C. Flemings, "Measurement of Microporosity by Microradiography", Transactions AIME, v. 233, 1965, pp. 355-359.

13. T. Z. Kattamis, M. C. Flemings, "Dendrite Morphology, Microsegregation, and Homogenization of Low Alloy Steel", Transactions AIME, v. 233, 1965, pp. 992-999.

14. M. C. Flemings, "Controlled Solidification", Proceedings of the Twelfth Sagamore Army Materials Research Conference, Strengthening Mechanisms, J. Burke, N. Reed, V. Weiss Editors. Syracuse University Press, 1966.

15. M. C. Flemings, "Application of Theory to Solidification of Large Castings and Ingots". Proceedings Joint Conference on the Solidification of Metals, Brighton, England, December 4-7, 1967 (to be published).

16. M. C. Flemings, D. R. Poirier, R. V. Barone, H. D. Brody, "Microsegregation in Iron Base Alloys" (to be published).

17. D. R. Poirier, "Activity of Carbon in Liquid Fe-C-Cr Solutions", Transactions AIME, v. 242, pp. 349-351.

18. D. R. Poirier, "Activity of Carbon in Austenite", Transactions AIME, v. 242, pp. 685-690.

19. H. Wentrup, "Die Bildung von Einschlüssen im Stahl", Technische Mitteilungen Krupp, Heft 5, 1937, pp. 131-142.

20. R. Vogel, W. Hotop, "Das Zustandsschaubild Eisen-Eisensulfid-Mangan", Archiv für das Eisenhüttenwesen, v. 11, 1937, pp. 41-45.

21. E. Schürmann, "Die Manganentschwefelung bei Gusseisen", Giesserei, Heft 17, 1961, pp. 481-487.

22. C. E. Sims, "A Review of Metallurgical Practices and their Effects" Electric Furnace Steel Proceedings, v. 10, 1952, p. 152.

23. C. E. Sims, C. W. Briggs, "The Effect of Various Deoxidizers on Cast Steels", 25th International Foundry Congress, Liège-Brussels, 1958.

24. L. Van Vlack, O. Riegger, R. Warrick, J. Dahl, "Sulfide Inclusions in Steel", Trans. AIME, v. 221, 1961, pp. 220-228.

25. R. Kiessling, C. Westman, "Sulfide Inclusions and Synthetic Sulfides of the (Mn, Me)S Type", Jour. Iron and Steel Inst., v. 204, 1966, pp. 377-379.

26. R. Kiessling, B. Hässler, C. Westman, "Selenide-Sulfide Inclusions and Synthetic Compounds of the (Mn, Me)(S,Se) Type", Jour. Iron and Steel Inst., v. 205, Part 5, 1967, pp. 531-534.

27. R. Kiessling, N. Lange, "Intergranular Brittleness of Cast Chromium-Nickel Steels", v. 201, 1963, pp. 761-762.

28. R. Kiessling, N. Lange, "Non-Metallic Inclusions in Steel", Part II, Publication No. 100, The Iron and Steel Institute, 1966.

29. K. Matsubara, "The Electron Microprobe", Proc. Symp. Electrochem. Soc. Wash. D. C., October 1964, pp. 632-641.

30. F. W. Boulger, "The Effect of Se on the Machinability and Tensile Properties of 5 Per Cent Chromium Steel", Trans. ASM, v. 52, 1960, pp. 698-712.

31. R. Gaydos, "Free Machining Steels and Effects of Sulfide and Siliceous Non-Metallics", Jour. Metals, v. 16, 1964, pp. 972-977.

32. P. Detrez, "Rôle de l'Oxygène, de l'Azote et de l'Aluminium sur la Qualité des Aciers Moulés", Fonderie, v. 229, 1965, pp. 73-86.

33. P. Detrez, "Illustration du Mechanisme de Formation des Sulfures", Fonderie, v. 247, 1966, pp. 333-338.

34. T. Araki, H. Hirai, K. Matsushita, T. Karasudani, "On the Behavior of Sulfide and Selenide Inclusions Formed in Steel Containing Cr and Mo", Tetsu-to-Hagané Overseas, v. 5, No. 2, June 1965, pp. 112-122.

35. D. A. Melford, P. Ducumb, "The Application of X-Ray Scanning Microanalysis to Some Metallurgical Problems", Metallurgia, v. 61, 1960, pp. 205-211.

36. E. J. Lichy, G. C. Duderstadt, N. L. Samways, "Control of Sulfide Shape in Low-Carbon Aluminum Killed Steel", Jour. Metals, v. 17, No. 7, 1965, pp. 769-775.

37. L. Bäcker, M. Rolin, C. Messager, "La Nature et la Composition des Sulfures dans les Aciers au Soufre à Usinabilité Ameliorée", Mém. Scient. Revue de Métallurgie, v. 63, No. 4, 1966, pp. 319-328.

38. M. Kondo, M. Osawa, T. Arai, S. Kumangai, "On the Inclusions in the Sulfurized High-Speed Steel", Jour. Japan. Inst. of Metals, v. 30, 1966, pp. 449-454.

39. T. Araki, H. Hirai, T. Karasudani, "Effect of Mo, C etc. on Sulfide Inclusions in Low Carbon Steel, I. Study of Behavior of Inclusions in Free Cutting Steel", Transactions Natl. Res. Inst. Metals, Tokyo, v. 7, No. 2, 1965, pp. 46-51.

40. P. H. Salmon Cox, J. A. Charles, "Further Observations on the Analysis and Distribution on Non-Metallic Inclusions in a 0.2%C Steel Ingot", Jour. Iron and Steel Inst., v. 203, 1965, pp. 493-499.

41. V. Karmazin, Stal, 5-6, 1940, pp. 24-30.

42. Whiteley, 3rd Report, Iron and Steel Inst., Heterogeneity Committee, 1929.

43. W. Nicodemi, "Effect of Cooling Rate on Non-Metallic Inclusions and Their Morphology in Stainless Steel Castings", Fonderia Italiana, v. 14, No. 12, 1965, pp. 473-479.

44. H. Hirai, T. Araki, S. Matsukuma, Y. Kojima, "Preliminary Experiments on Rate of Solidification and the Formation of Sulfide Inclusions in Resulfurized Steels", Tetsu-to-Hagané, v. 51, No. 4, 1965, pp. 816-819 (Brutcher No. 6695).

45. R. B. G. Yeo, "The Effect of Oxygen on Resulfurized Steels, Parts I and II", Jour. Metals, v. 19, 1967, pp. 29-32 (June) and pp. 23-27 (July).

46. W. Dahl, H. Hangstemberg, C. Düren, "Conditions for the Occurrence of the Various Types of Sulfide Inclusions", Stahl und Eisen, v. 86, 1966, No. 13, pp. 782-795.

47. W. Crafts, D. C. Hilty, "Sulfide and Oxide Formation in Steel", Proceedings of Electric Furnace Steel Conference, 1953, pp. 121-150.

48. J. E. Hilliard, J. W. Cahn, "An Evaluation of Procedures in Quantitative Metallography for Volume Fraction Analysis", Transactions AIME, v. 221, 1961, pp. 344-352.

49. G. A. Chadwick, Eutectic Alloy Solidification, Pergamon Press, Oxford, 1963.

50. M. Hansen, Constitution of Binary Alloys, McGraw-Hill, New York, 1958.

51. E. T. Turkdogan, S. Ignatowicz, J. Pearson, "Solubility of Sulfur in Iron and Iron-Manganese Alloys", Jour. Iron and Steel Inst., v. 180, 1955, pp. 349-354.

52. T. Z. Kattamis, M. C. Flemings, "Solidification of Highly Undercooled Castings", Modern Casting, v. 52, No. 1, 1967, pp. 191-198.

53. M. Myers, Department of Metallurgy and Materials Science, M.I.T., Private Communication.

54. J. C. Yarwood, Department of Metallurgy and Materials Science, M.I.T., Private Communication.

55. D. C. Hilty, "Influence of Sulfur on Oxygen Solubility in Steel", Jour. Metals, v. 18, 1966, pp. 201-204.

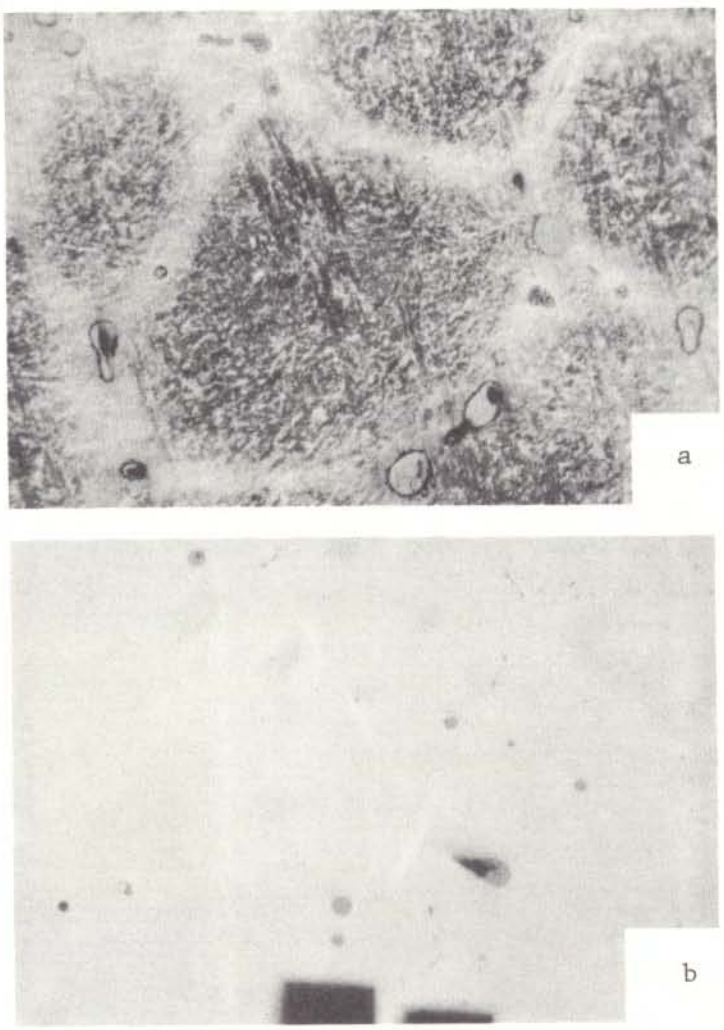

Figure 1: Photomicrograph of AISI 4330 - 0.1% S specimen, solidified at 40°C/min. (a) Etched, 300X. Type I sulfide inclusions. (b) Unetched, 200X. Mixed Type I-II sulfide inclusions.

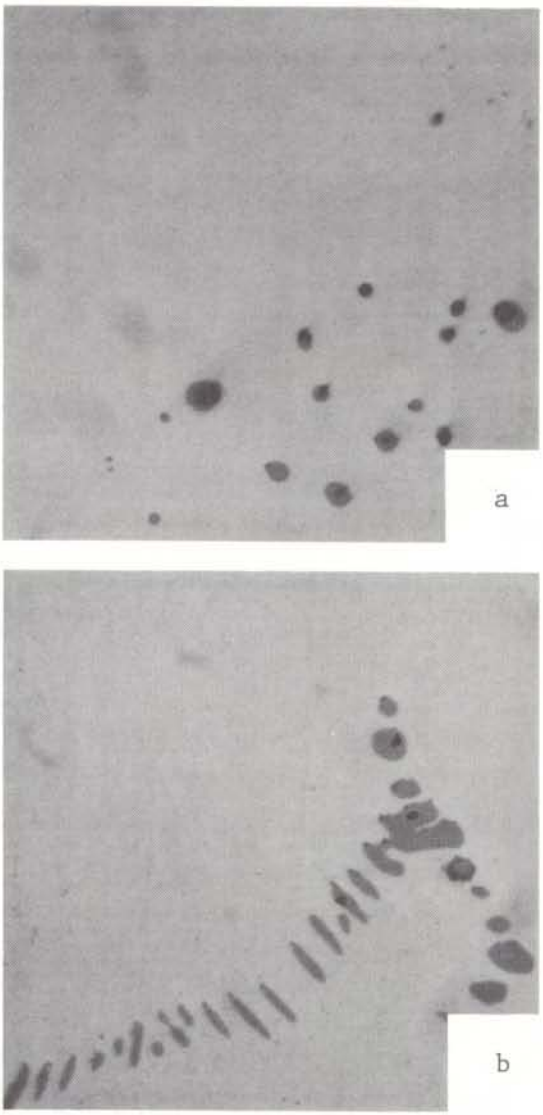

Figure 2: Photomicrographs of two AISI 4330 specimens containing 0.01% S and 1.0% S, respectively, solidified at 40°C/min, 1000X.
(a) Type I sulfide inclusions,
(b) Type II sulfide inclusions

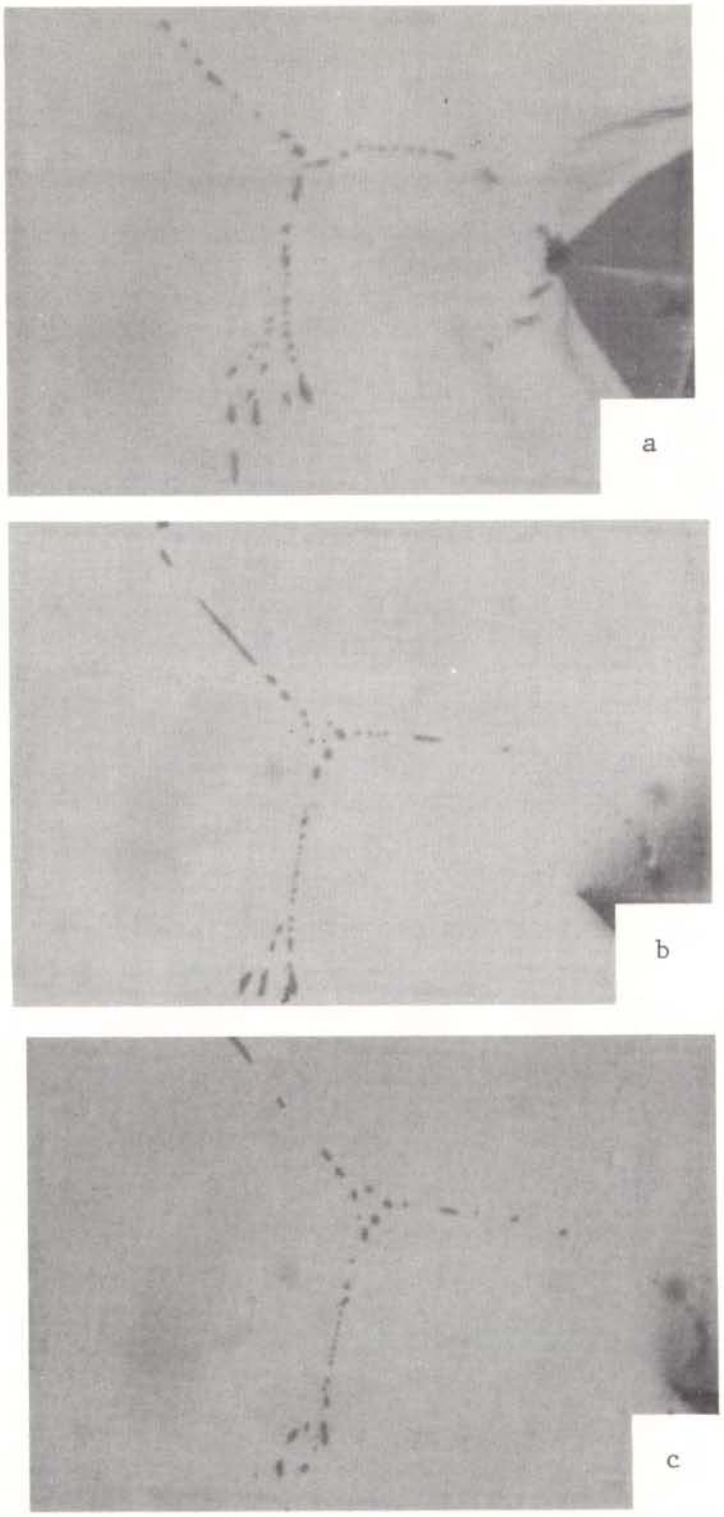

Figure 3: Photomicrographs of an AISI 4330-0.1%S specimen, solidified at 70°C/min, 200X. Unetched, showing inclusion morphology on successive surfaces obtained by polishing down the specimen. Note how inclusions that appear rod-like in one section, appear as beads in another section. Sections approximately 200 microns apart.

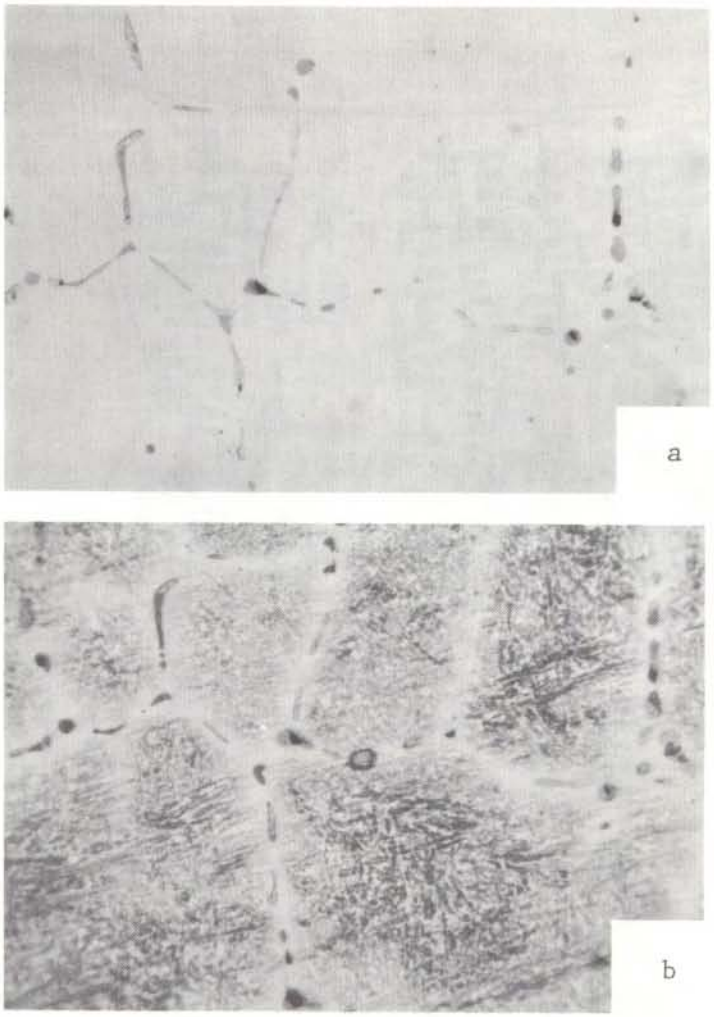

Figure 4: Photomicrographs of AISI 4330-0.1% S specimen, 250X. (a) Unetched, (b) Same area, etched with Rosenhain's reagent, showing Type II inclusions aligned along dendrite arm boundaries.

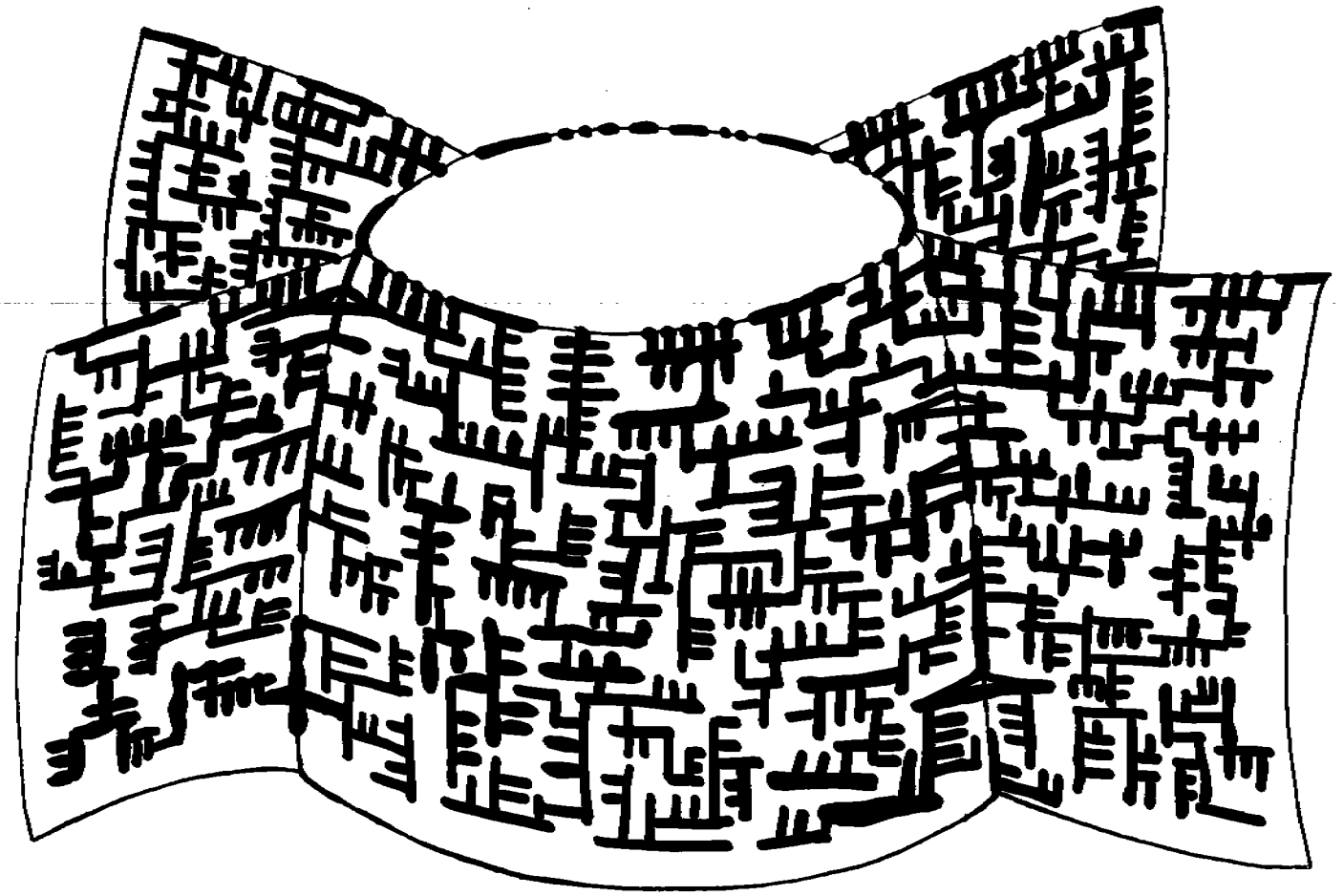

Figure 5: Schematic representation of a case of Type II eutectic inclusions at dendrite arm boundaries.

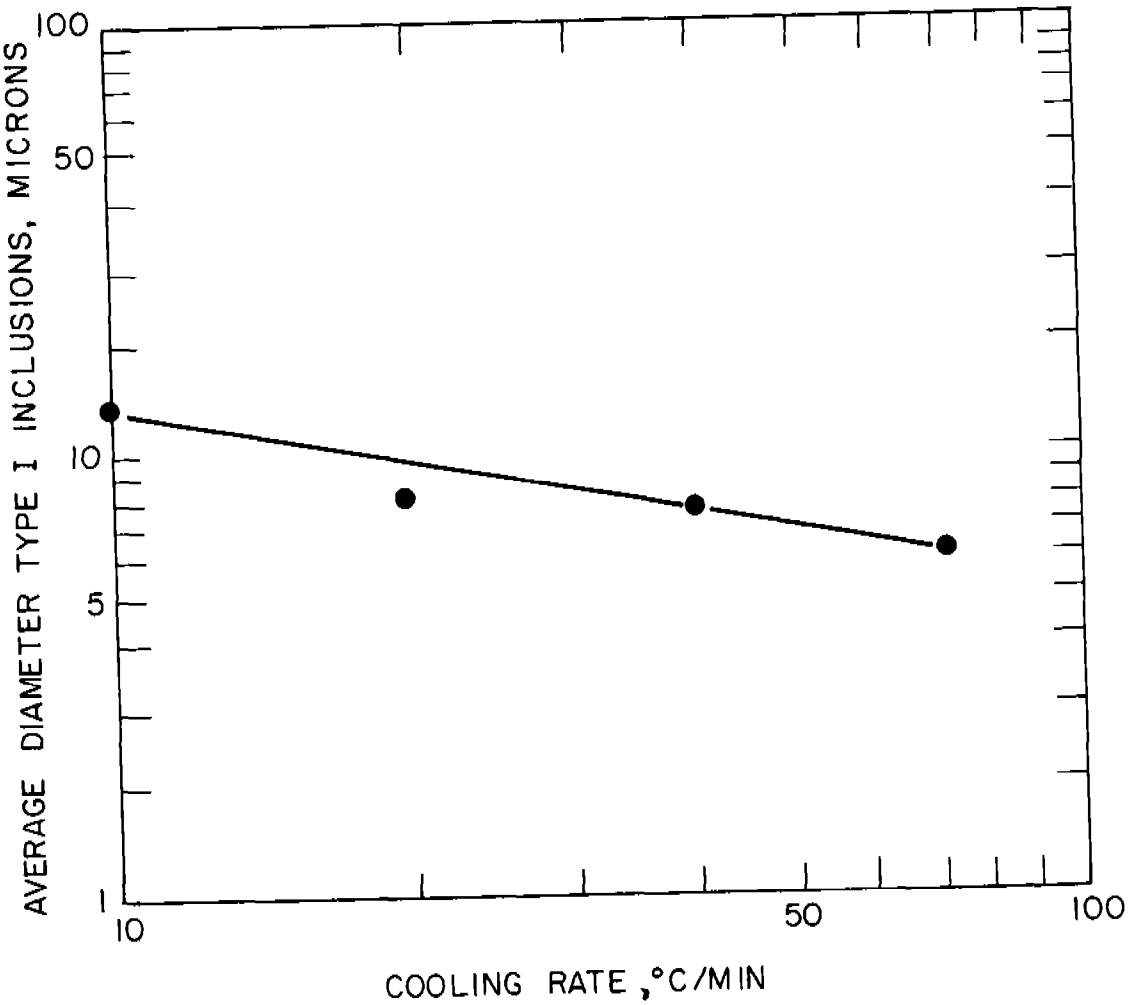

Figure 6: Average diameter of Type I sulfide inclusions versus cooling rate. AISI 4330 - 0.1% S specimens.

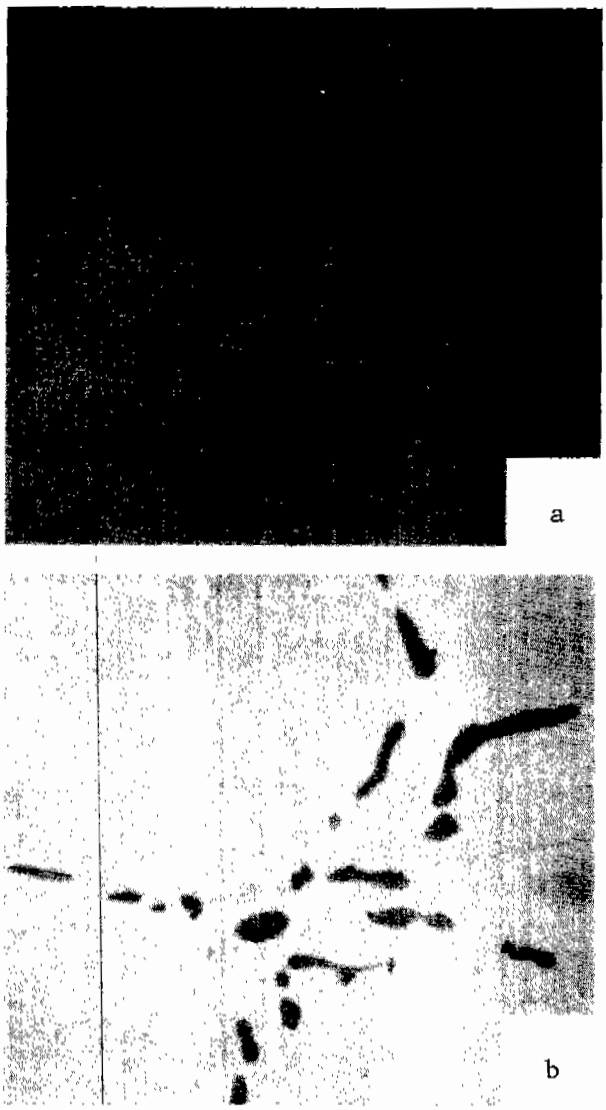

Figure 7: Photomicrographs of AISI 4330-0.1% S showing finer Type II eutectic inclusions at higher cooling rate, 500X. Cooling rates are: (a) 70°C/min., (b) 10°C/min.

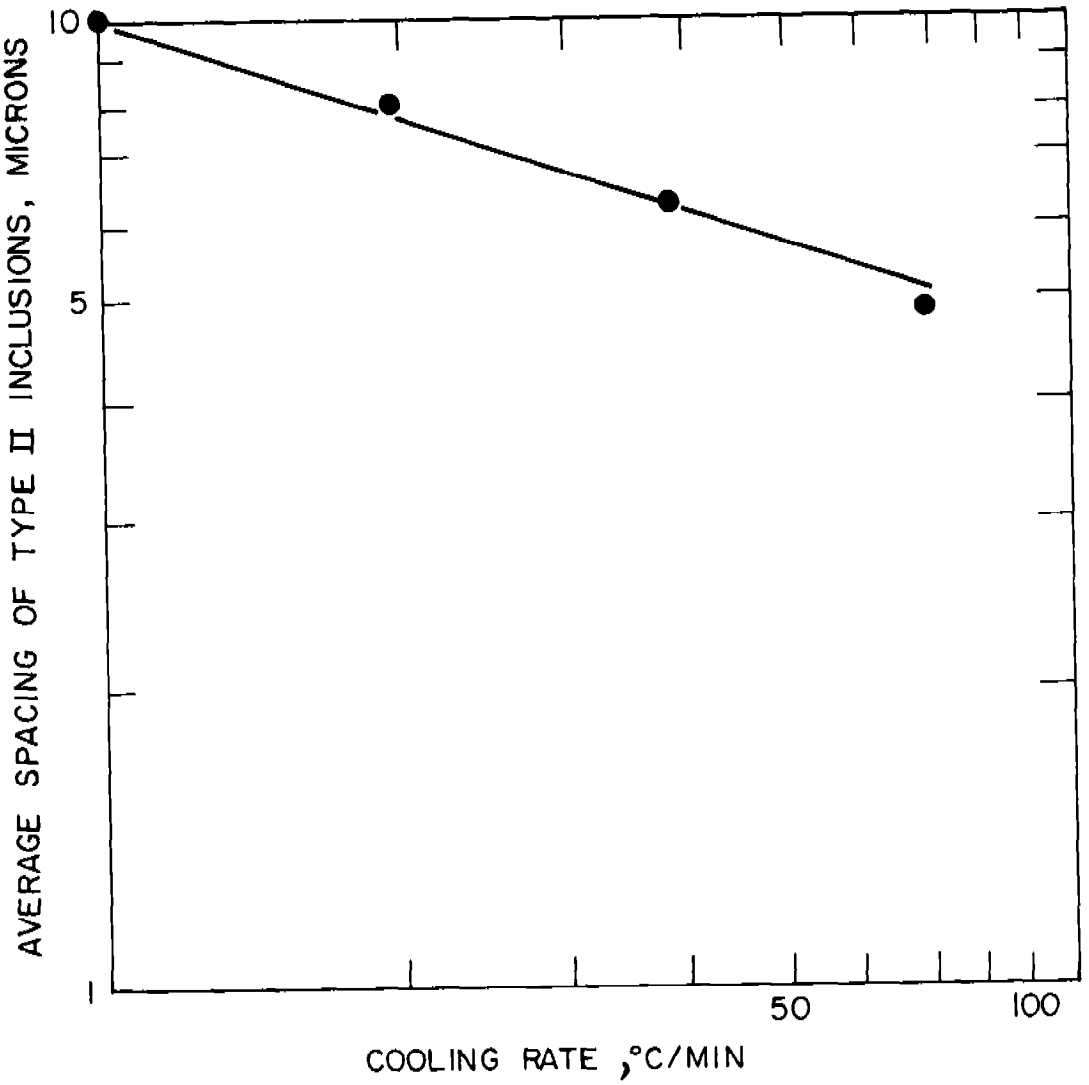

Figure 8: Average spacing of Type II eutectic inclusions versus cooling rate. AISI 4330 - 0.1% S specimens.

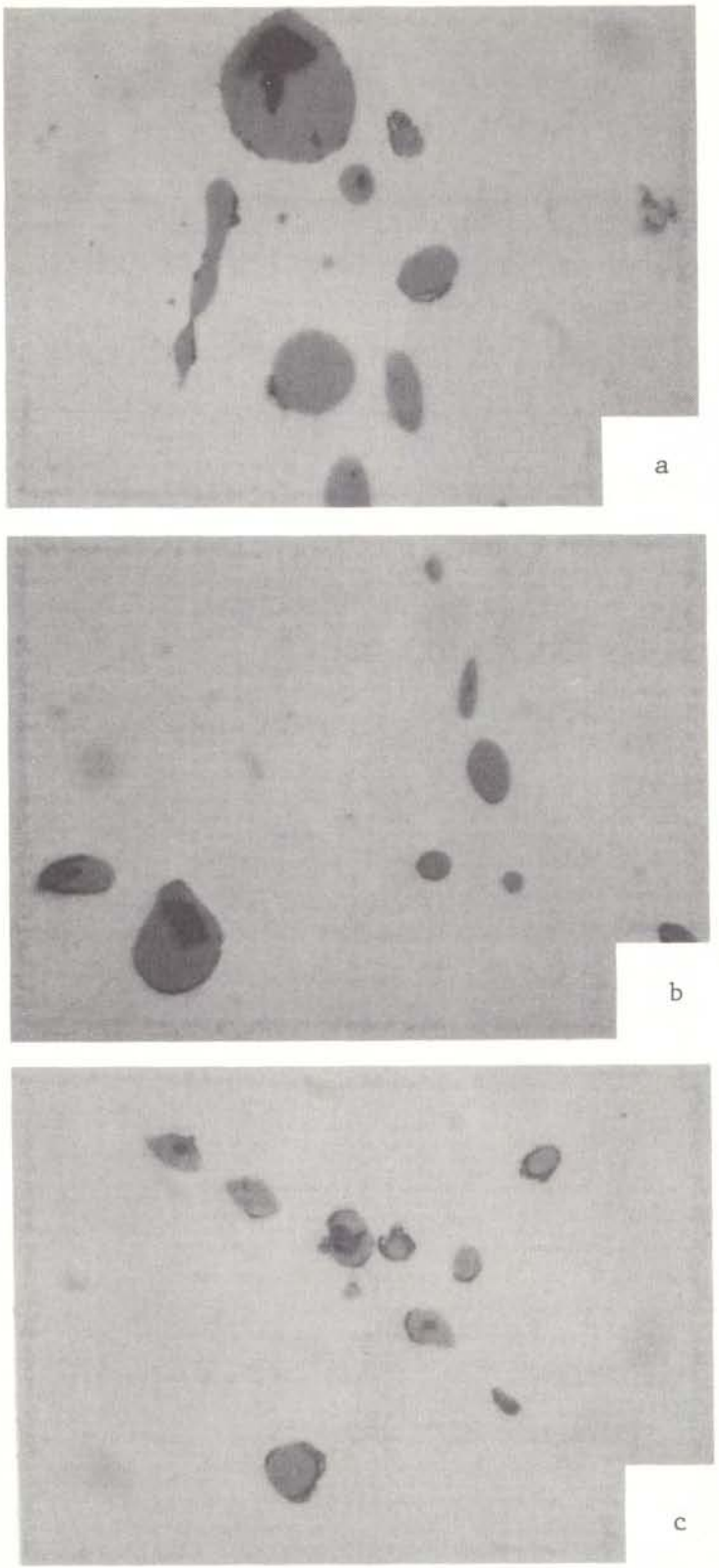

Figure 9: Photomicrographs of AISI 4330-0.1% S - 0.08% O specimen solidified at 40°C/min, 1000X. (a) Center of the Ingot, (b) region at half distance between center and edge of the ingot, (c) edge of the ingot.

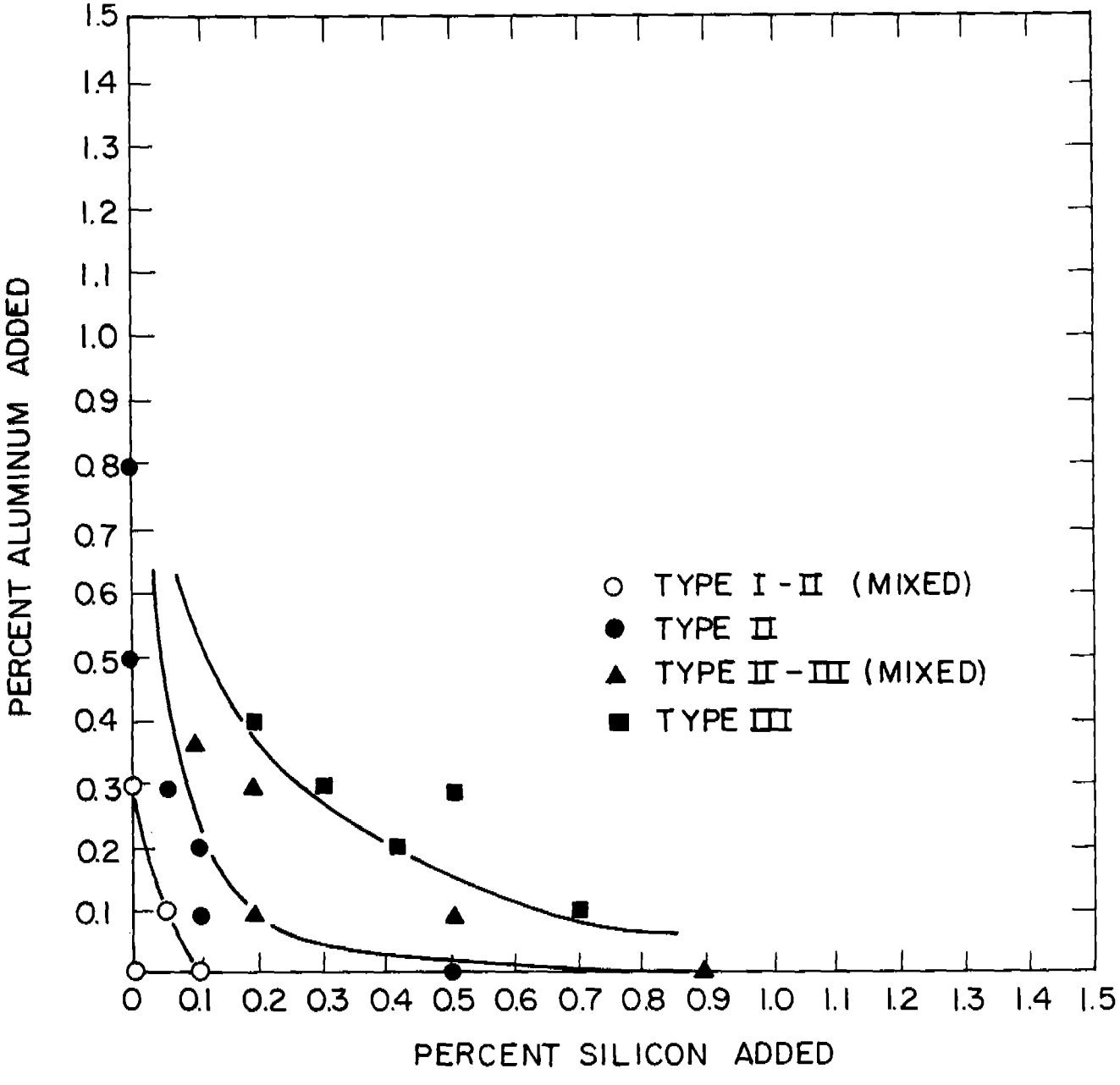

Figure 10: Type of sulfide inclusions versus Al and Si additions. AISI 4330 - 0.1% S specimens solidified at 40°C/min.

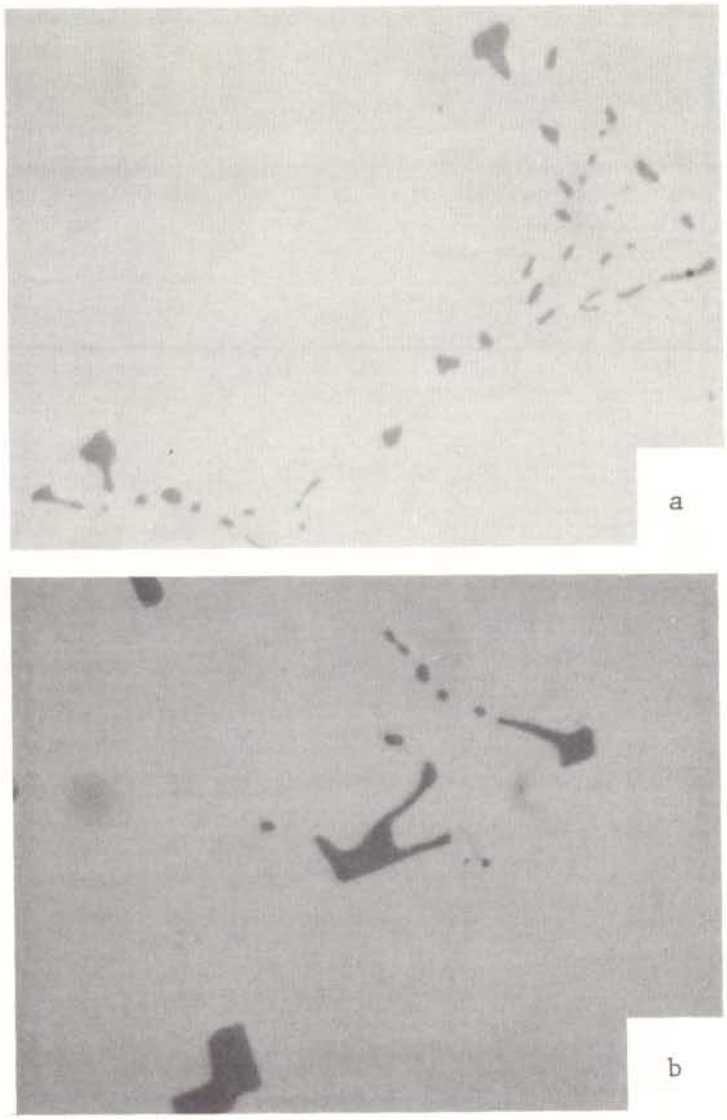

Figure 11: Photomicrographs of AISI 4330-0.1% S - 0.2% Si - 0.3% Al specimen solidified at 40°C/min. Mixed Type II-III sulfide inclusions. (a) 500X, (b) 1000X.

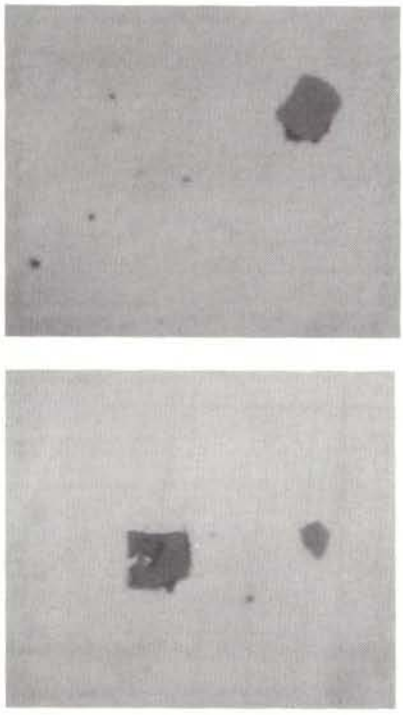

Figure 12: Photomicrographs of AISI 4330-0.1%S-0.2%Si-0.4%Al specimen solidified at 40°C/min,500X. Type III sulfide inclusions.

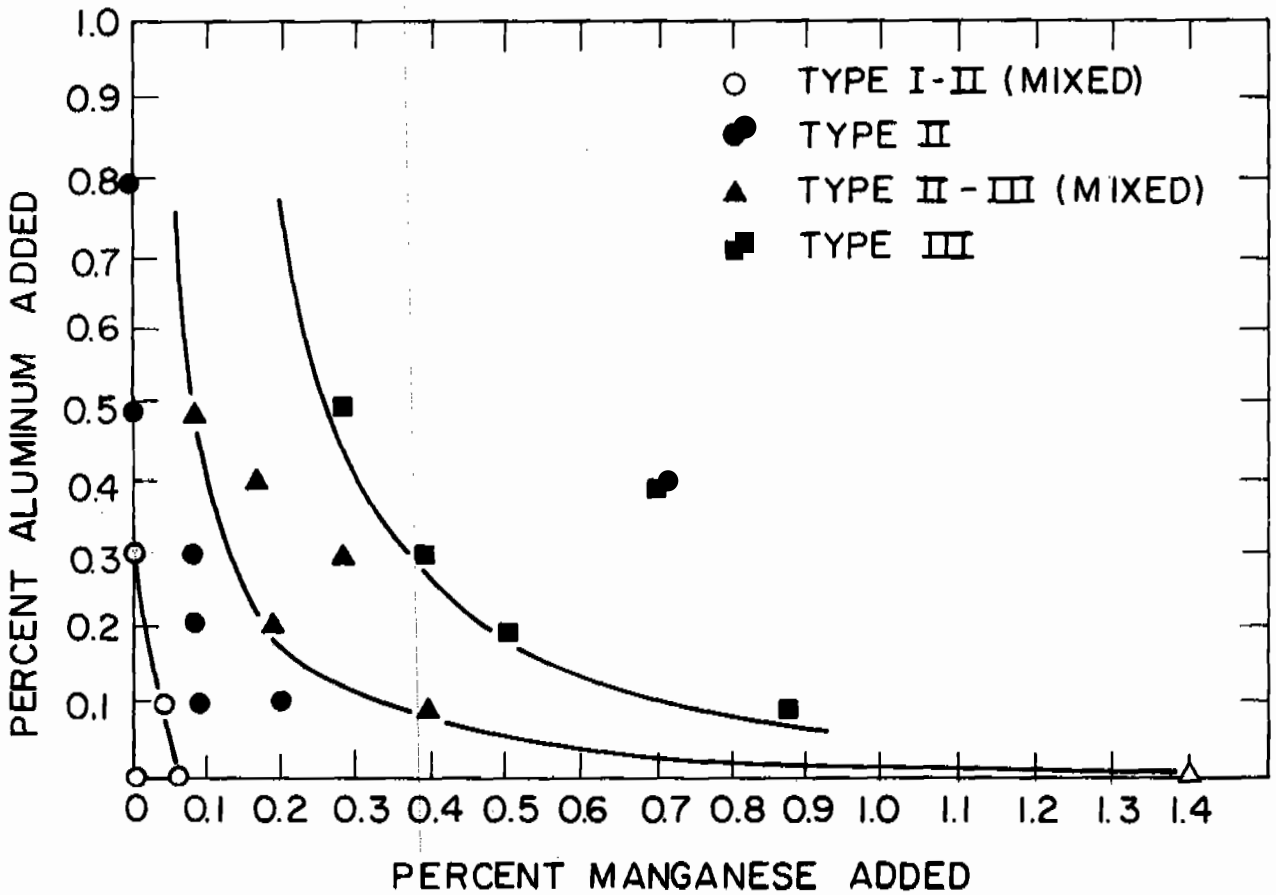

Figure 13: Type of sulfide inclusions versus Al and Mn additions. AISI 4330 - 0.1% S specimens solidified at 40°C/min.

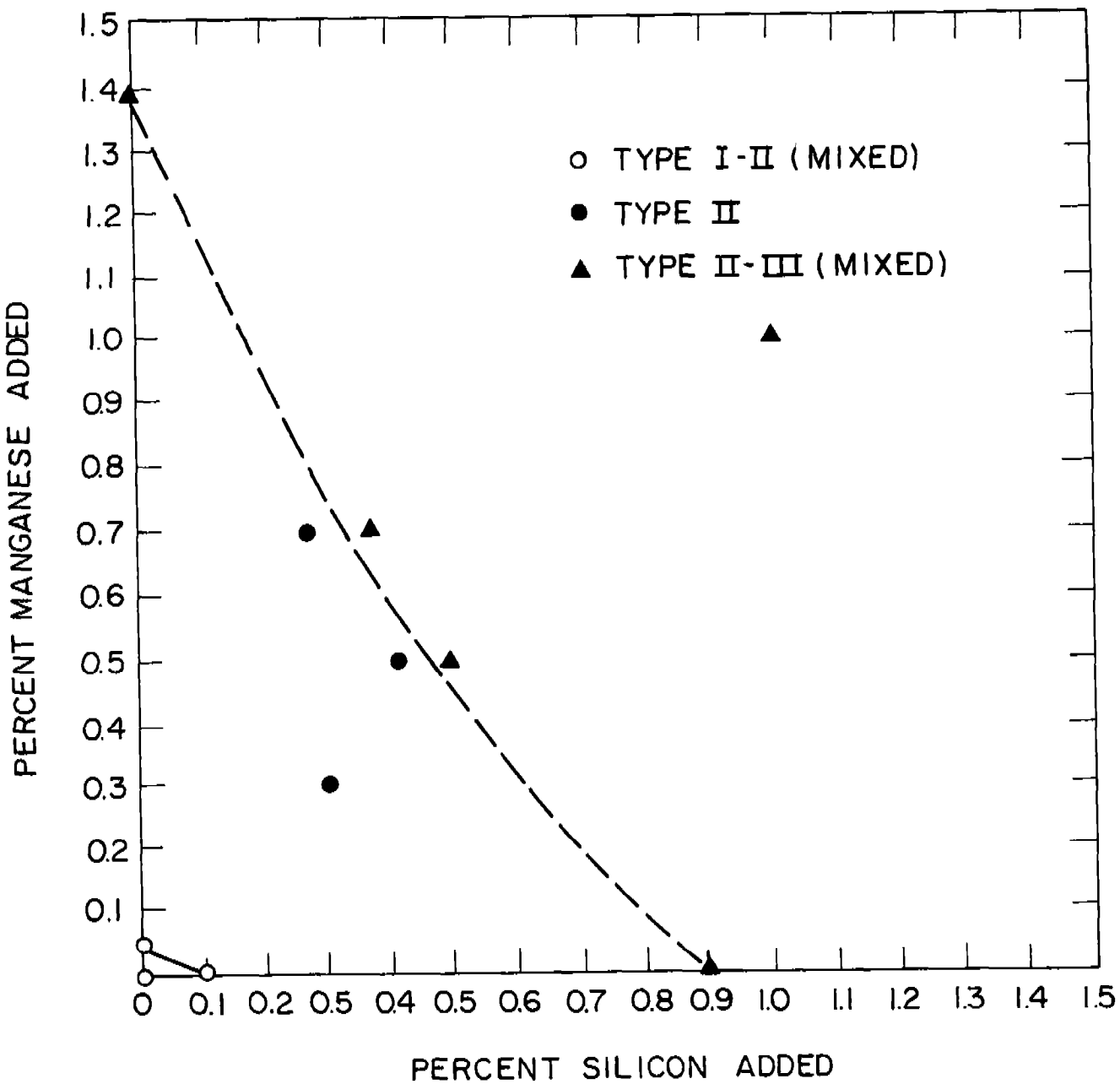

Figure 14: Type of sulfide inclusions versus Mn and Si additions. AISI 4330 - 0.1% S specimens solidified at 40^{0}C/min.

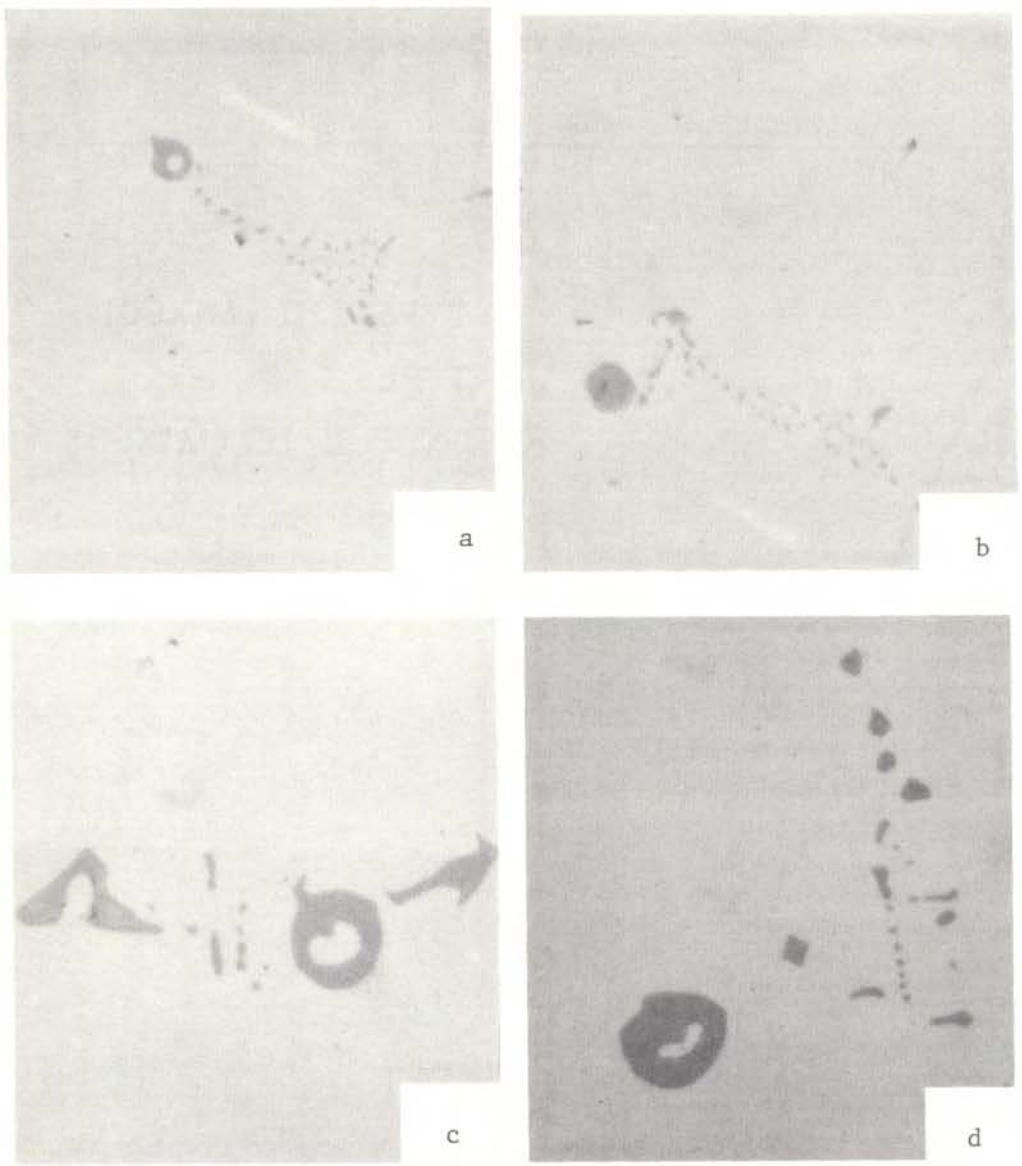

Figure 15: Photomicrographs of AISI 4330-0.1% S - 0.3% Mn - 0.3% Si specimen solidified at 40°C/min, showing Type I ring-like sulfide inclusions adjacent to Type III and Type II inclusions. (a) 500X , (b) 500X, (c) 1000X, (d) 1000X.

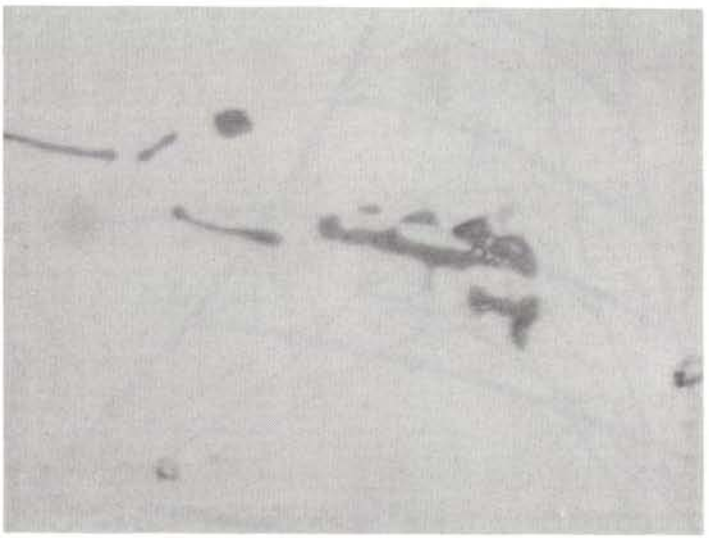

Figure 16: Photomicrograph of AISI 4330 - 0.1% S - 0.3% Si- 0.3% Mn specimen solidified at 40°C/min, 1000X. Type II sulfide inclusions showing internal eutectic structure.

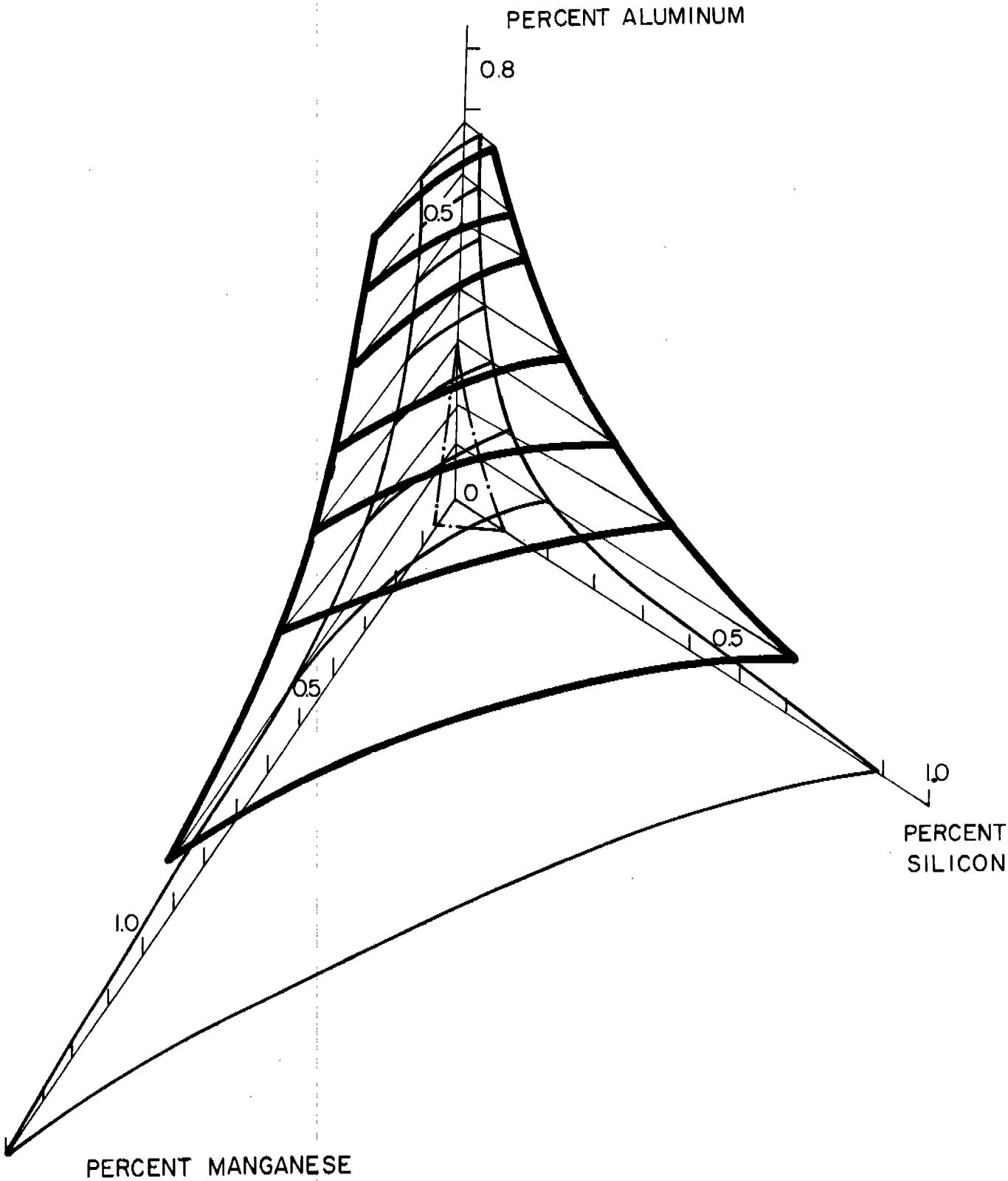

Figure 17: Type of sulfide inclusions versus Al,Mn,and Si additions.
AISI 4330 - 0.1% S specimens solidified at 40°C/min.

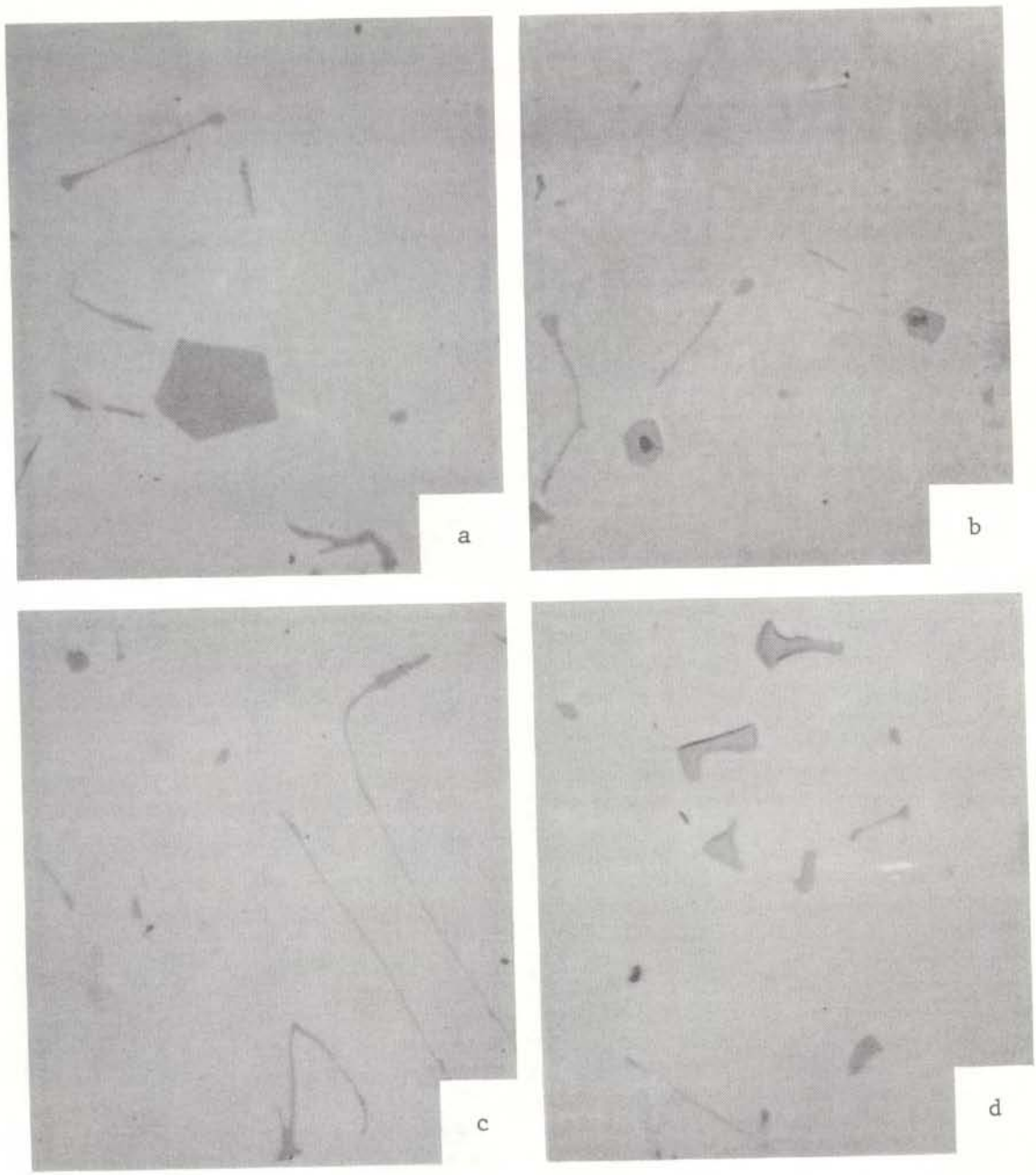

Figure 18: Photomicrographs of AISI 4330 - 0.1% S - 0.4% Zr specimen solidified at 40°C/min, 500X. (a), (b), and (c) show sulfide inclusions, (d) shows zirconium silicate inclusions (Z) adjacent to sulfide inclusions (S).

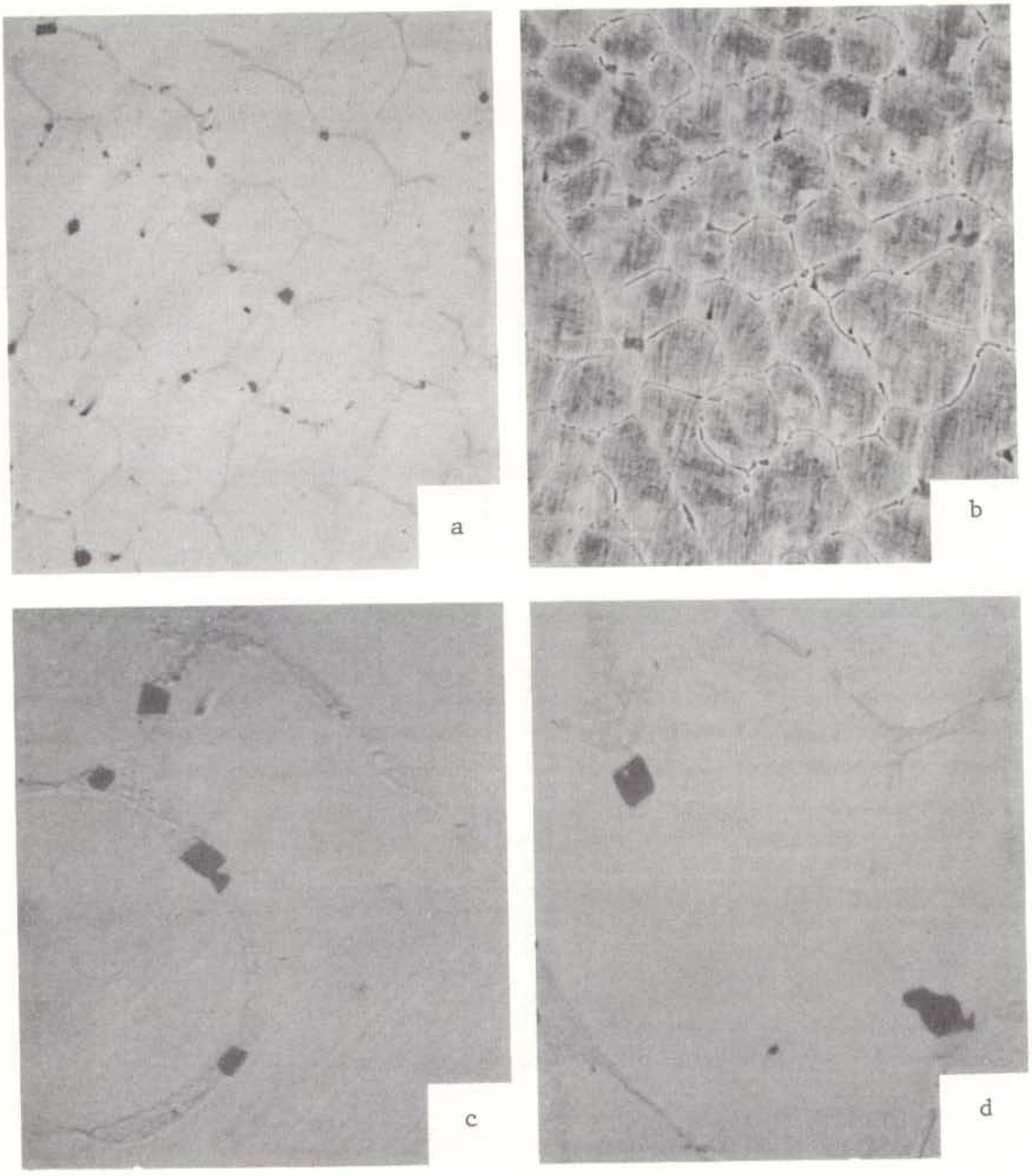

Figure 19: Photomicrographs of AISI 4330 - 0.1% S - 0.3% B specimen solidified at 40°C/min, (a) unetched, 200X, (b) etched, 200X, (c) and (d) unetched, 500X.

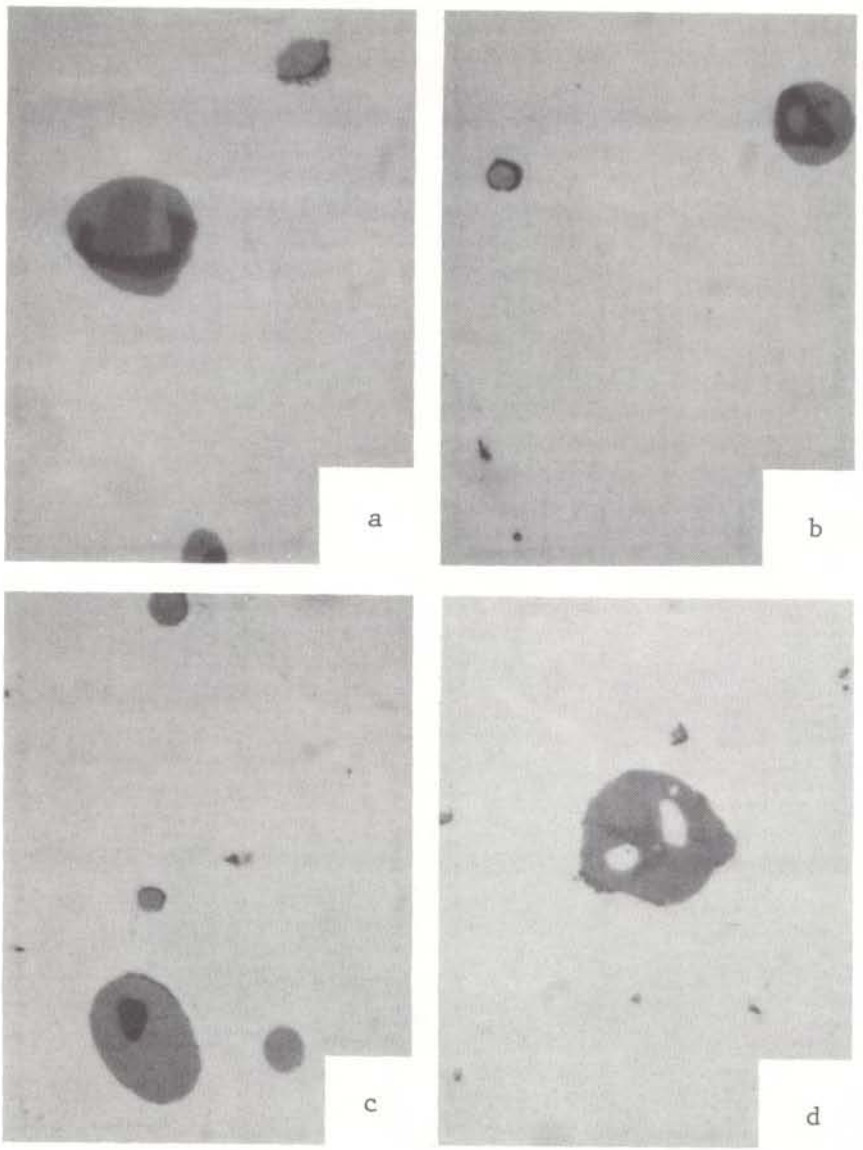

Figure 20: Photomicrograph of AISI 4330 - 0.1% S - 0.1% Ce specimen solidified at 40°C/min, 1000X. Unetched. Type I multiphase sulfide inclusions.

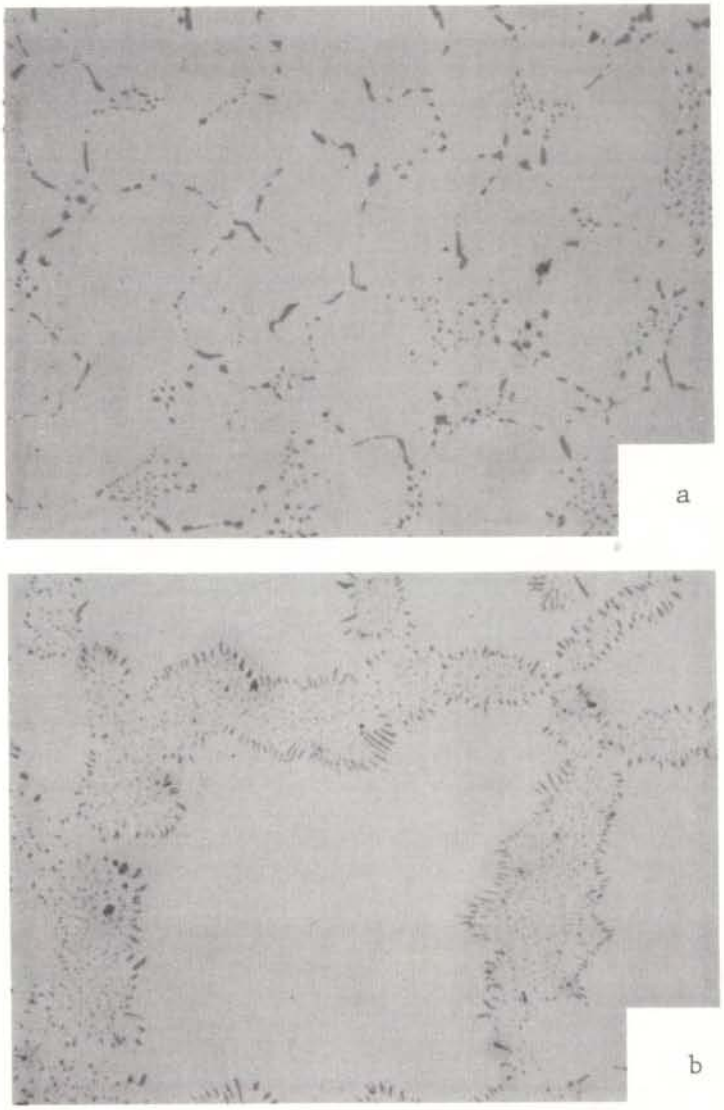

Figure 21: Photomicrographs of AISI 4330 - 0.5% S - 2% Mn specimen solidified at 40°C/min, showing mixed Type I-II sulfide inclusions. (a) 200X, (b) a different region, 500X.

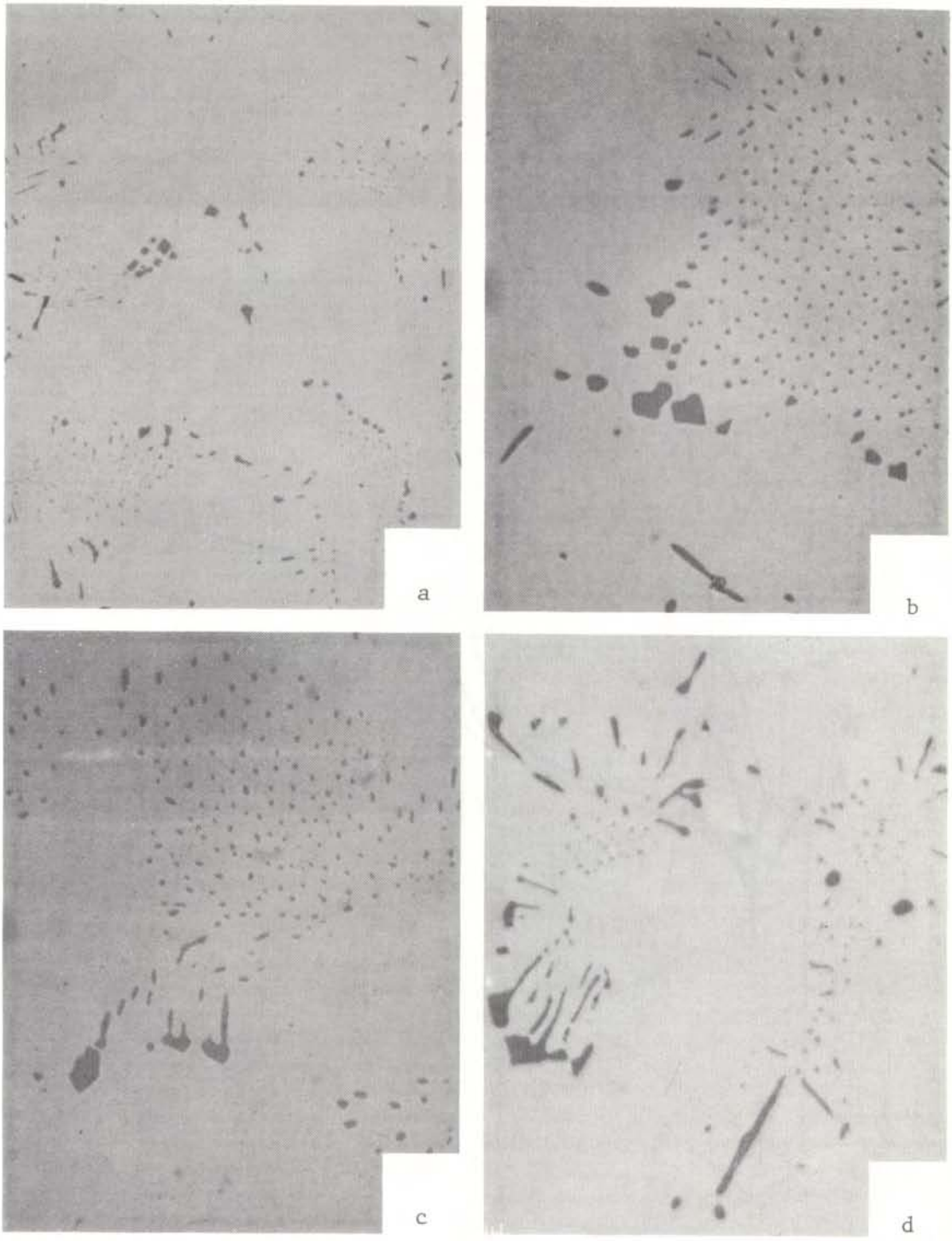

Figure 22: Photomicrographs of AISI 4330 - 0.5% S - 2%Mn - 0.3% Si specimen solidified at 40^{o}C/min showing mixed Type II-III inclusions. (a) 200X; (b),(c),and (d) 500X.

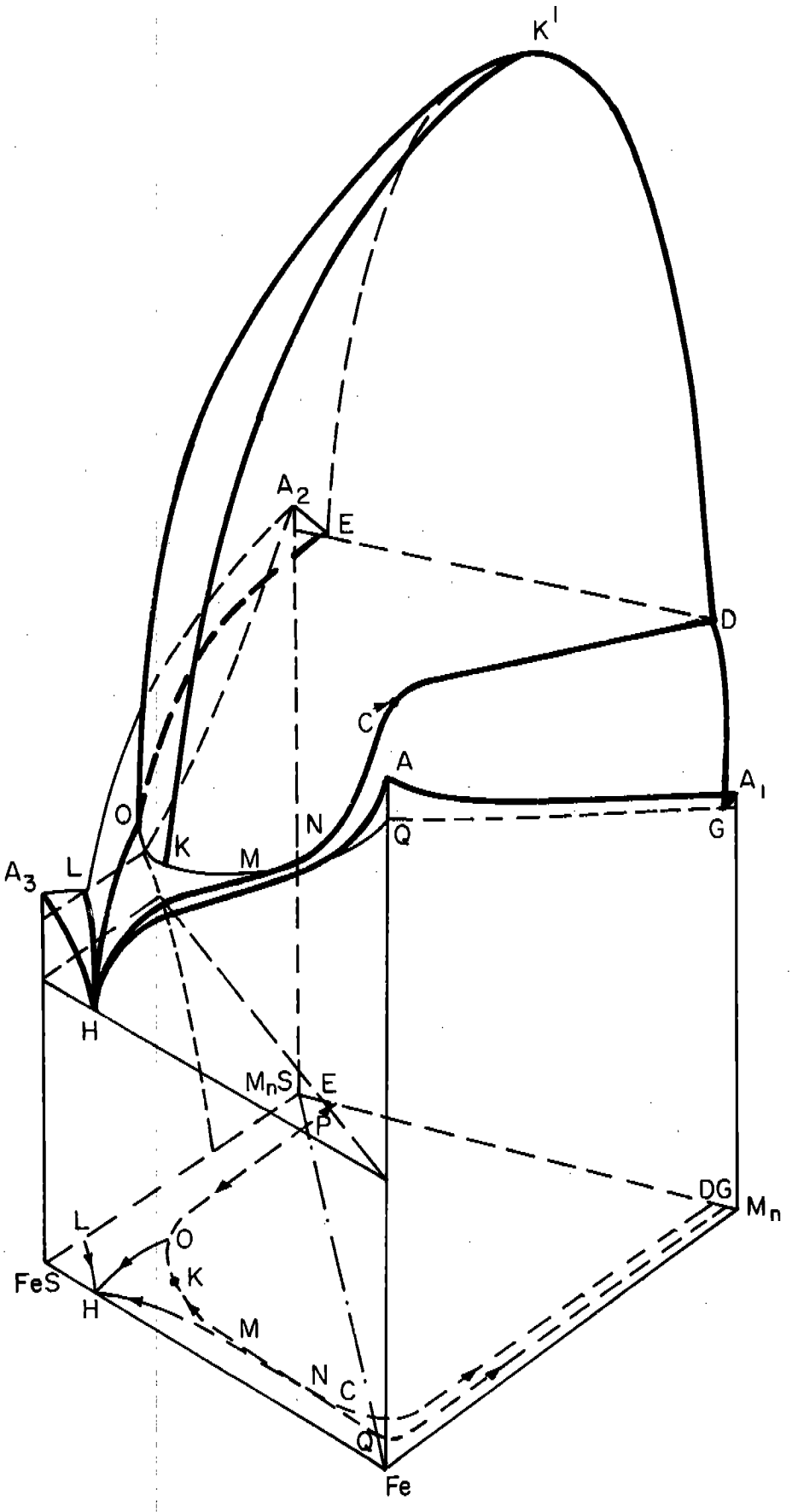

Figure 23: Schematic representation of the Fe - Mn - FeS - MnS part of the Fe - Mn - S phase diagram.

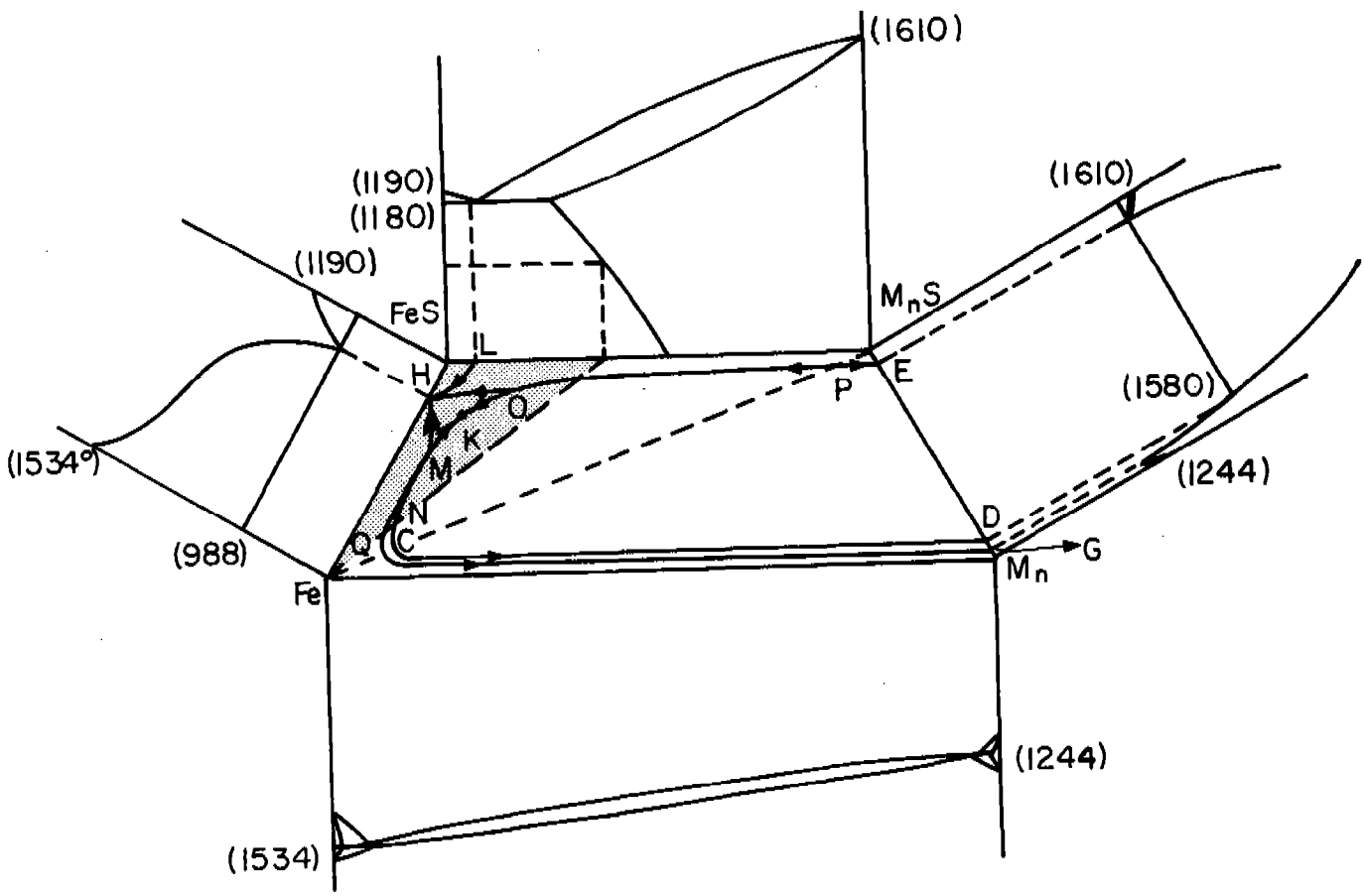

Figure 24: The four binary phase diagrams of the Fe - Mn - FeS - MnS system and the basal projection of the three eutectic valleys and of the contour limiting the miscibility gap. The projection of the ternary eutectic plane appears shadowed.

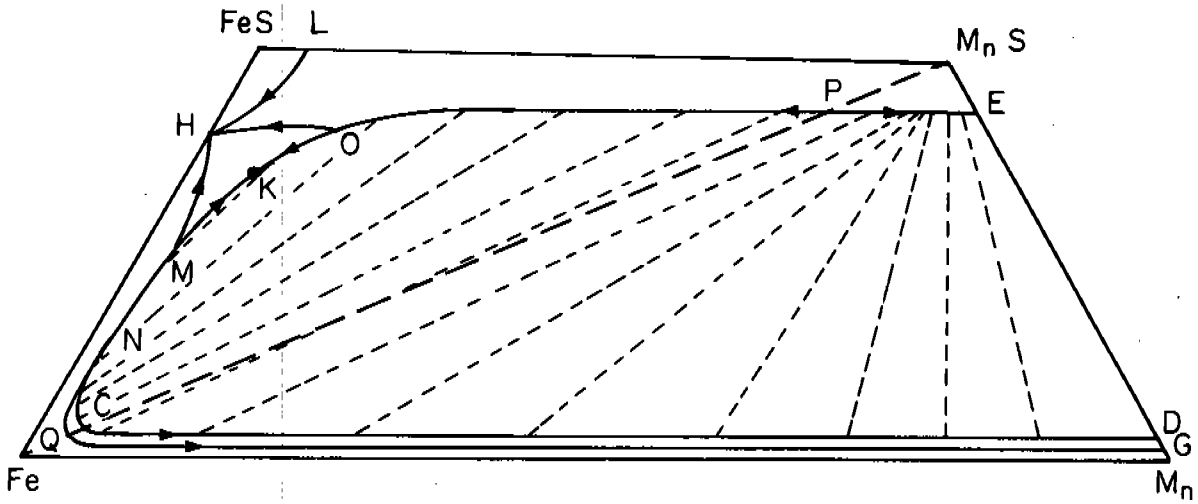

(a)

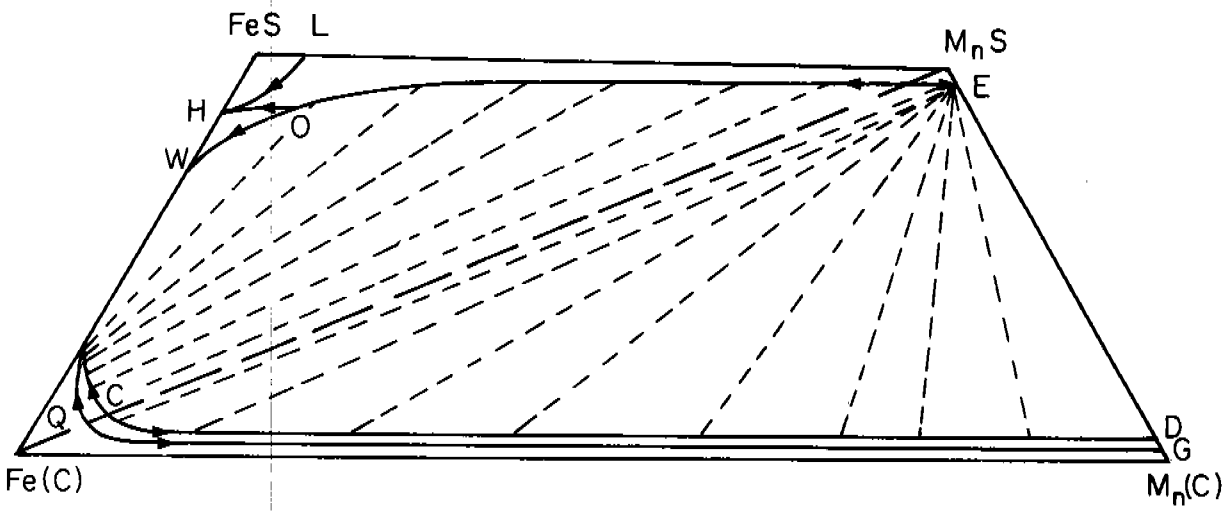

(b)

Figure 25: (a) Basal projection of the Fe - Mn- S system showing the miscibility gap,tie lines across the gap,and the eutectic valleys. (b) Basal projection of the Fe(C saturated) -Mn- S system indicating the shifting of the miscibility gap,of the tie lines across the gap and of the eutectic valleys.

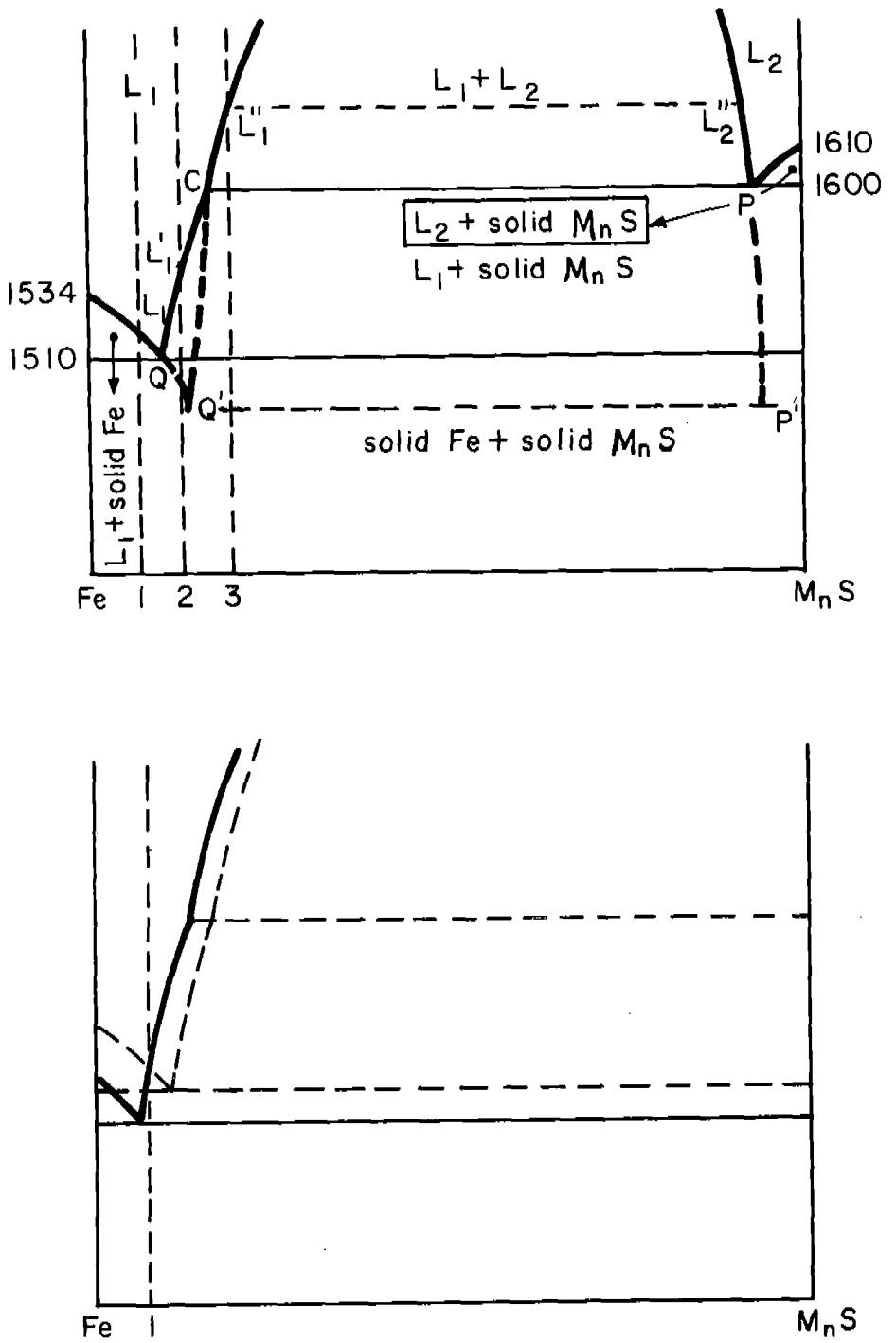

Figure 26: (a) Schematic representation of the pseudo-binary Fe - MnS phase diagram obtained by sectioning the ternary Fe - Mn-S phase diagram by the vertical plane whose trace on the basal plane is the diagonal Fe - MnS. (b) Schematic shifting of the equilibrium lines between the various phases by addition of deoxidizers.

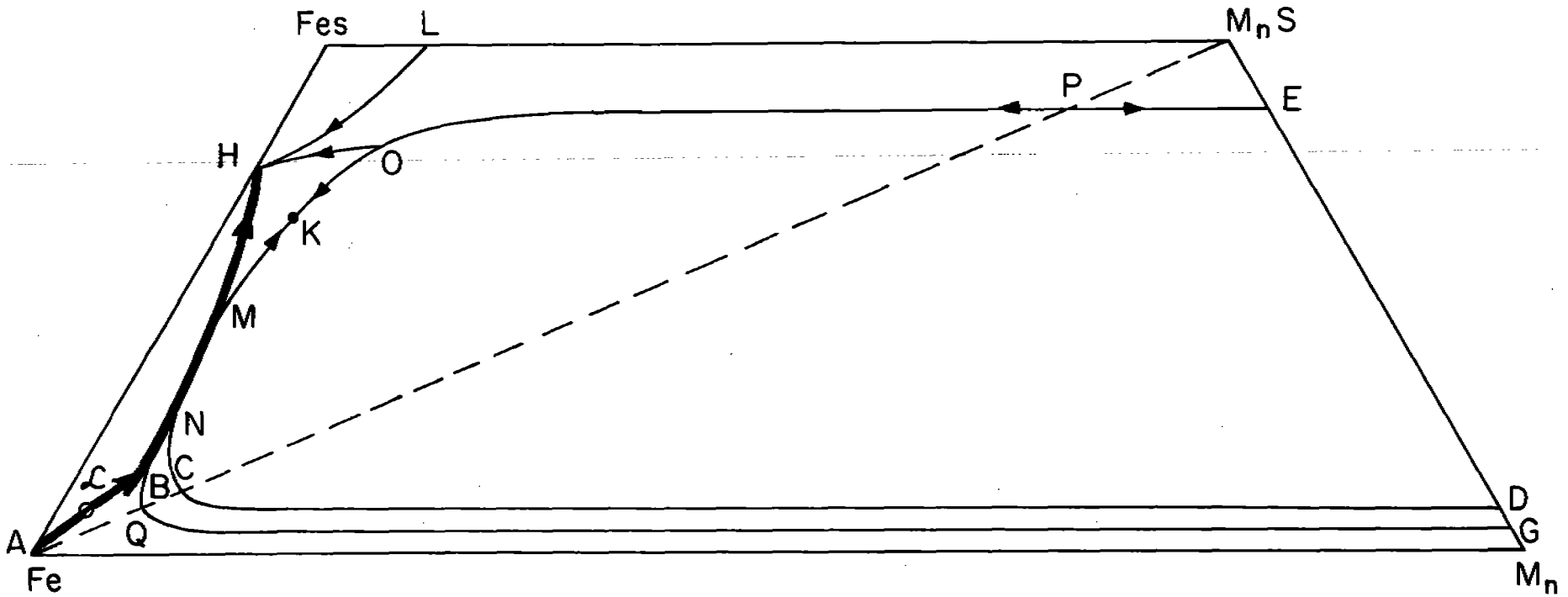

Figure 27: Schematic representation of the solidification path of melt $\mathcal{L}$.

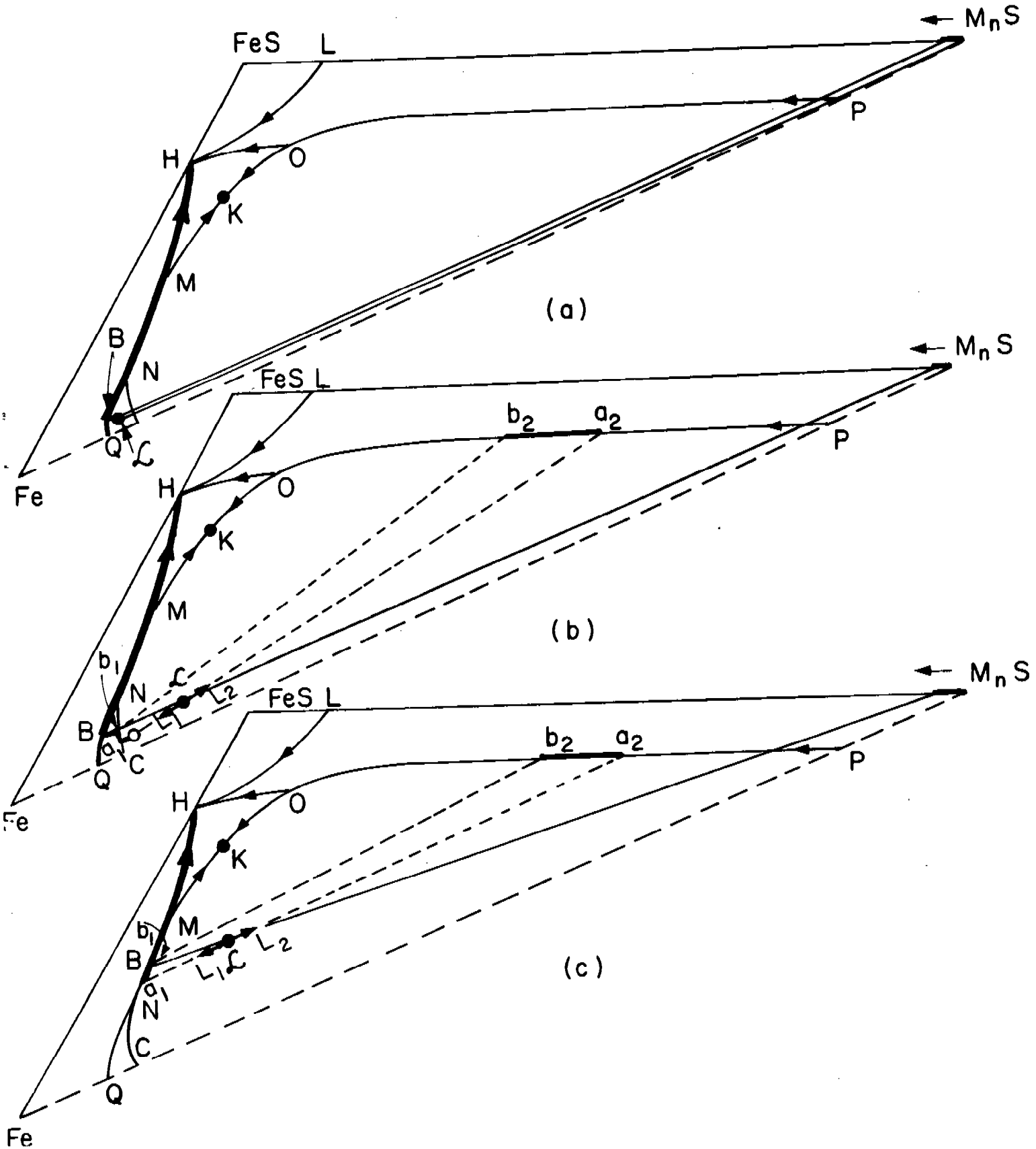

Figure 28: Schematic representation of the solidification paths of three different melts $\mathcal{L}$.

DISTRIBUTION LIST

	No. of Copies
Office of the Director Defense Research and Engineering The Pentagon Washington,D.C. 20301	
Attn: Mr. J.C.Barrett	1
Dr. Donald MacArthur	1
Commander Defense Documentation Center Cameron Station,Bldg. 5 5010 Duke Station Alexandria,Virginia 22314	20
Defense Metals Information Center Battelle Memorial Institute Columbus,Ohio 43201	2
National Aeronautics and Space Administration Washington,D.C. 20546	
Attn: Mr. B.G.Achhammer	1
Mr. G.C.Deutsch	1
Mr. R.V.Rhode	1
National Aeronautics and Space Administration Marshall Space Flight Center Huntsville,Alabama 35812	
Attn: R-P & VE-M,Dr. W. Lucas	1
M-F & AE-M,Mr. W.A.Wilson,Bldg.4720	1
Chief of Research and Development Department of the Army Washington,D.C. 20310	
Attn: Physical and Engineering Science Division	2
Headquarters Aeronautical Systems Division Wright-Patterson Air Force Base,Ohio 45433	
Attn: AFML (MAA)	2
AFML (MAT)	1
AFML (MAM)	1
AFML (MAN)	1

DISTRIBUTION LIST

	No. of Copies
Chief Office of Naval Research Department of the Navy Washington, D. C. 20360 Attn: Code 423	1
Commander U. S. Naval Research Laboratory Anacostia Station Washington, D. C. 20390 Attn: Technical Information Office	1
Commanding General Deseret Test Center Fort Douglas, Utah 84113 Attn: Technical Information Office	1
Commanding General U. S. Army Electronics Command Fort Monmouth, New Jersey 07703 Attn: AMSEL-RD-M	2
Commanding General U. S. Army Materiel Command Washington, D. C. 20315 Attn: AMCRD-RC-M	1
Commanding General U. S. Army Missile Command Redstone Arsenal, Alabama 35809 Attn: Technical Library	1
Commanding General U. S. Army Munitions Command Dover, New Jersey 07801 Attn: Technical Library	1
Commanding General U. S. Army Tank-Automotive Center Warren, Michigan 48090 Attn: Tech Data Coord. Br., SMOTA-RTS SMOTA-RCM.1	2 1
Commanding General U. S. Army Weapons Command Rock Island, Illinois 61201 Attn: Research & Development Directorate, AMSWE-RDR	1

DISTRIBUTION LIST

	No. of Copies
Commanding General U. S. Army Satellite Communications Agency Fort Monmouth, New Jersey 07703 Attn: Technical Document Center	1
Commanding General White Sand Missile Range White Sands, New Mexico 88002 Attn: STEWS-WS-VT	1
Commanding Officer Aberdeen Proving Ground Maryland 21005 Attn: Technical Library, Bldg. 313	1
Commanding Officer U. S. Army Research Office (Durham) Box CM Duke Station Durham, North Carolina 27706	1
Commanding Officer Frankford Arsenal Bridge and Tacony Street Philadelphia, Pennsylvania 19137 Attn: Library Branch, C-2500 Mr. H. Markus, SMUFA-L7000	1 1
Commanding Officer Picatinny Arsenal Dover, New Jersey 07801 Attn: SMUPA-VA6	1
Commanding Officer Watervliet Arsenal Watervliet, New York 12189 Attn: SWEWV-RDT, Technical Information Services Offices	1
Commanding Officer U. S. Army Aviation Materiel Laboratories Fort Eutstis, Virginia 23604	1
Commanding Officer USACDC Ordnance Agency Aberdeen Proving Ground, Maryland 21005 Attn: Library, Bldg. 305	2

	No. of Copies
Commanding Officer U. S. Army Edgewood Arsenal Edgewood Arsenal, Maryland 21010 Attn: Dir. of Eng. & Ind. Serv., Chem-Mun Br., (Mr. F. E. Thompson)	1
Redstone Scientific Information Center U.S. Army Missile Command Redstone Arsenal, Alabama 35809 Attn: Chief, Documents Section	4
U. S. Army Aviation School Library USAAVNS-P&NRI Fort Rucker, Alabama 36360	1
Department of the Army Ohio River Division Laboratories Corps of Engineers 5851 Mariemont Avenue Cincinnati, Ohio 45227 Attn: ORDLB-TR	1
Commanding Officer Army Materials and Mechanics Research Center Watertown, Massachusetts 02172 Attn: AMXMR-AT, Technical Information Branch AMXMR-AA AMXMR-MX, Mr. N. Reed AMXMR-RX, Dr. R. Beeuwkes, Jr. AMXMR-RP, Mr. G. A. Darcy, Jr. AMXMR-TP, Mr. P. A. G. Carbonaro AMXMR-TP, Castings and Cermets Branch	5 1 1 1 1 1 5
American Foundrymen's Society Golf and Wolf Roads Des Plaines, Illinois 60016 Attn: Mr. P. R. Gouwens	1
Case Institute of Technology University Circle Cleveland, Ohio 44106 Attn: Professor J. F. Wallace	1
Dartmouth College Thayer School of Engineering Hanover, New Hampshire 03755 Attn: Professor G. A. Colligan	1
Harvard University Cambridge, Massachusetts 02139 Attn: Professor Bruce Chalmers	1

DISTRIBUTION LIST

	No. of Copies
Investment Casting Institute 3525 West Peterson Road Chicago, Illinois 60645 Attn: Mr. R. E. Pritchard	1
Massachusetts Institute of Technology Cambridge, Massachusetts 02139 Attn: Professor M. C. Flemings	1
Northeastern University 360 Huntington Avenue Boston, Massachusetts 02115 Attn: Professor John Zotos	1
Steel Founders' Society Westview Towers 21010 Center Ridge Road Rocky River, Ohio 44116 Attn: Mr. Charles Briggs	1
Tufts University Medford, Massachusetts 02155 Attn: Professor K. Van Wormer, Jr.	1

AD Accession No.

U. S. Army Materials Research Agency, Watertown, Massachusetts 02172
INVESTIGATION OF SOLIDIFICATION OF HIGH-STRENGTH STEEL CASTINGS
T.Z.Kattamis,and M.C.Flemings

Report AMMRC CR 63-04/6, October 1966-December 1967,67 pp-tables-illus,AMCMS Code No. 5025.11.294,D/A Project No.1C024401A328,
Unclassified Report

The morphology,size and distribution of sulfide inclusions are studied in vacuum melted and solidified AISI 4330 low alloy steel deoxidized with various elements such as Al,Si,Mn,either individually or in various combinations,and B,Zr,and Ce. Types I,II and III inclusions are investigated in detail. Type I inclusions are isolated,roughly spherical sulfides,Type II inclusions have interconnected rod-like morphology,and Type III inclusions are angular and unconnected (except they are often connected to Type II inclusions).

Effects of chemistry (Al,Si,Mn) on inclusion type is quantitatively determined. The effect of cooling rate on inclusion type and size is examined for a few cases With decreasing cooling rate,the average size of Type I inclusions and the average spacing of the eutectic Type II inclusions increase.

The origin of the various types of inclusions observed is interpreted with the aid of the Fe-MnS pseudo-binary phase diagram and the Fe-Mn-S ternary phase diagram. Modifications of these diagrams from addition of the various deoxidizers are qualitatively predicted and taken into account. It is concluded that Type I inclusions form by exsolution of liquid sulfide pools from the melt,Type III inclusions form by solidification of sulfide crystals out of the melt and Type II inclusions form by eutectic solidification of the sulfur-rich final liquid. Interpretation of structures observed suggests that Type I and possibly Type III inclusions are "pushed" ahead of the growing dendrites. Morphology of inclusions is adequately predicted on the basis of only temperature and mode of solidification; such factors as surface energy differences between different inclusions types need not be postulated to explain their different morphologies.

NO DISTRIBUTION LIMITATIONS

UNCLASSIFIED

1. Cast Steel
2. Solidification
3. Sulfide Inclusions
4. Fe-Mn-S Phase Diagram
5. Deoxidation

I. T.Z.Kattamis, M.C.Flemings

II. AMCMS Code No.

III. D/A Project

UNCLASSIFIED

Security Classification

DOCUMENT CONTROL DATA - R&D

(Security classification of title, body of abstract and indexing annotation must be entered when the overall report is classified)

1. ORIGINATING ACTIVITY (Corporate author)

Massachusetts Institute of Technology
Cambridge, Massachusetts 02139

2a. REPORT SECURITY CLASSIFICATION

Unclassified

2b. GROUP

3. REPORT TITLE

INVESTIGATION OF SOLIDIFICATION OF HIGH-STRENGTH STEEL CASTINGS

4. DESCRIPTIVE NOTES (Type of report and inclusive dates)

Interim Report - October 1, 1966- December 31,1967

5. AUTHOR(S) (Last name, first name, initial)

T. Z. Kattamis, and M. C. Flemings

6. REPORT DATE	7a. TOTAL NO. OF PAGES	7b. NO. OF REFS
July 15,1968	67	55

8a. CONTRACT OR GRANT NO.	9a. ORIGINATOR'S REPORT NUMBER(S)
DA-19-020-AMC-5443(X)	AMMRC CR 63-04/F
b. PROJECT NO. D/A 1C024401A328	9b. OTHER REPORT NO(S) (Any other numbers that may be assigned this report)
c. AMCMS Code 5025.11.294	
d.	

10. AVAILABILITY/LIMITATION NOTICES

This Document has been Approved for Public Release and Sale; Its Distribution is Unlimited.

11. SUPPLEMENTARY NOTES	12. SPONSORING MILITARY ACTIVITY
	U.S. Army Materials Research Agency Watertown, Massachusetts 02172

13. ABSTRACT

See attached sheet.

DD FORM 1 JAN 64 1473

UNCLASSIFIED

Security Classification

14. KEY WORDS	LINK A		LINK B		LINK C	
	ROLE	WT	ROLE	WT	ROLE	WT
Cast Steel Solidification Sulfide Inclusions Fe-Mn-S Phase Diagram Deoxidation						

INSTRUCTIONS

1. ORIGINATING ACTIVITY: Enter the name and address of the contractor, subcontractor, grantee, Department of Defense activity or other organization *(corporate author)* issuing the report.

2a. REPORT SECURITY CLASSIFICATION: Enter the overall security classification of the report. Indicate whether "Restricted Data" is included. Marking is to be in accordance with appropriate security regulations.

2b. GROUP: Automatic downgrading is specified in DoD Directive 5200.10 and Armed Forces Industrial Manual. Enter the group number. Also, when applicable, show that optional markings have been used for Group 3 and Group 4 as authorized.

3. REPORT TITLE: Enter the complete report title in all capital letters. Titles in all cases should be unclassified. If a meaningful title cannot be selected without classification, show title classification in all capitals in parenthesis immediately following the title.

4. DESCRIPTIVE NOTES: If appropriate, enter the type of report, e.g., interim, progress, summary, annual, or final. Give the inclusive dates when a specific reporting period is covered.

5. AUTHOR(S): Enter the name(s) of author(s) as shown on or in the report. Enter last name, first name, middle initial. If military, show rank and branch of service. The name of the principal author is an absolute minimum requirement.

6. REPORT DATE: Enter the date of the report as day, month, year; or month, year. If more than one date appears on the report, use date of publication.

7a. TOTAL NUMBER OF PAGES: The total page count should follow normal pagination procedures, i.e., enter the number of pages containing information.

7b. NUMBER OF REFERENCES: Enter the total number of references cited in the report.

8a. CONTRACT OR GRANT NUMBER: If appropriate, enter the applicable number of the contract or grant under which the report was written.

8b, 8c, & 8d. PROJECT NUMBER: Enter the appropriate military department identification, such as project number, subproject number, system numbers, task number, etc.

9a. ORIGINATOR'S REPORT NUMBER(S): Enter the official report number by which the document will be identified and controlled by the originating activity. This number must be unique to this report.

9b. OTHER REPORT NUMBER(S): If the report has been assigned any other report numbers *(either by the originator or by the sponsor)*, also enter this number(s).

10. AVAILABILITY/LIMITATION NOTICES: Enter any limitations on further dissemination of the report, other than those imposed by security classification, using standard statements such as:

(1) "Qualified requesters may obtain copies of this report from DDC."

(2) "Foreign announcement and dissemination of this report by DDC is not authorized."

(3) "U. S. Government agencies may obtain copies of this report directly from DDC. Other qualified DDC users shall request through

_____."

(4) "U. S. military agencies may obtain copies of this report directly from DDC. Other qualified users shall request through

_____."

(5) "All distribution of this report is controlled. Qualified DDC users shall request through

_____."

If the report has been furnished to the Office of Technical Services, Department of Commerce, for sale to the public, indicate this fact and enter the price, if known.

11. SUPPLEMENTARY NOTES: Use for additional explanatory notes.

12. SPONSORING MILITARY ACTIVITY: Enter the name of the departmental project office or laboratory sponsoring *(paying for)* the research and development. Include address.

13. ABSTRACT: Enter an abstract giving a brief and factual summary of the document indicative of the report, even though it may also appear elsewhere in the body of the technical report. If additional space is required, a continuation sheet shall be attached.

It is highly desirable that the abstract of classified reports be unclassified. Each paragraph of the abstract shall end with an indication of the military security classification of the information in the paragraph, represented as *(TS), (S), (C), or (U).*

There is no limitation on the length of the abstract. However, the suggested length is from 150 to 225 words.

14. KEY WORDS: Key words are technically meaningful terms or short phrases that characterize a report and may be used as index entries for cataloging the report. Key words must be selected so that no security classification is required. Identifiers, such as equipment model designation, trade name, military project code name, geographic location, may be used as key words but will be followed by an indication of technical context. The assignment of links, rules, and weights is optional.

ABSTRACT

The morphology, size and distribution of sulfide inclusions are studied in vacuum melted and solidified AISI 4330 low alloy steel deoxidized with various elements such as Al, Si, Mn, either individually or in various combinations, and B, Zr and Ce. Types I, II and III inclusions are investigated in detail. Type I inclusions are isolated, roughly spherical sulfides, Type II inclusions have an interconnected rod-like morphology, and Type III inclusions are angular and unconnected (except they are often connected to Type II inclusions).

Effects of chemistry (Al, Si, Mn) on inclusion type is quantitatively determined. The effect of cooling rate on inclusion type and size is examined for a few cases. With decreasing cooling rate, the average size of Type I inclusions and the average spacing of the eutectic Type II inclusions increase.

The origin of the various types of inclusions observed is interpreted with the aid of the Fe-MnS pseudo-binary phase diagram and the Fe-Mn-S ternary phase diagram. Modifications of these diagrams from addition of the various deoxidizers are qualitatively predicted and taken into account. It is concluded that Type I inclusions form by exsolution of liquid sulfide pools from the melt, Type III inclusions form by solidification of sulfide crystals out of the melt and Type II inclusions form by eutectic solidification of the sulfur-rich final liquid. Interpretation of structures observed suggests that Type I and possibly Type III inclusions are "pushed" ahead of growing dendrites. Morphology of inclusions is adequately predicted on the basis of only temperature and mode of solidification; such factors as surface energy differences between different inclusion types need not be postulated to explain their different morphologies.